New Mesozoic and Cenozoic data help constrain the age of motion on the Altyn Tagh fault and rotation of the Qaidam basin.

Yan Chen, Stuart Gilder, Nadir Halim, Jean-Pascal Cogné, Vincent Courtillot

New paleomagnetic constraints on central Asian kinematics: Displacement along the Altyn Tagh fault and rotation of the Qaidam Basin

Yan Chen,[1] Stuart Gilder,[2] Nadir Halim,[3] Jean Pascal Cogné,[2] and Vincent Courtillot[2]

Received 23 July 2001; revised 9 January 2002; accepted 26 February 2002; published 5 October 2002.

[1] In order to better understand the tectonic evolution of central Asia under the influence of the India-Asia collision, we carried out a paleomagnetic study of 1500 cores from 106 sites along the Altyn Tagh fault, in the Qaidam and Tarim basins, and on the Tibetan plateau. Samples were mainly collected from Jurassic to Neogene siltstones and sandstones. In most cases stepwise thermal demagnetization unblocks low and high temperature components carried by magnetite and hematite. Low temperature components are north and down directed and lie close to the recent geomagnetic field. High temperature components from 10 of 13 age/locality groups pass fold and/or reversal tests and likely represent primary remanent magnetizations. The ten overall mean directions display a complex pattern of vertical-axis block rotations that are compatible with a tectonic model of clockwise rotation of the Qaidam Basin and concomitant left-lateral slip on the Altyn Tagh fault. Two of the ten localities are rotated significantly counterclockwise; they lie adjacent to the Altyn Tagh fault zone, consistent with the idea that left-lateral strike-slip motion occurred along it. The age of counterclockwise rotation near the eastern extremity of the fault was dated as younger than 19 Ma. Three widely spread areas within the Qaidam Basin exhibit similar and significant clockwise rotations, on the order of 20°, with respect to the North China Block, Tarim and Eurasia. The mean of the three values is thought to represent the total rotation of Qaidam. Because the youngest rocks displaying clockwise rotations are Oligocene, the main phase of Qaidam Basin rotation, and hence shear on the Altyn Tagh fault, took place after or near the end of the Oligocene (~24 Ma). Upper Neogene strata located on the Qaidam Basin are not significantly rotated, thus tectonic deformation acting since the Upper Neogene (~5 Ma) is not resolvable by paleomagnetic methods. Given a 20° ± 5° clockwise rotation of the Qaidam Basin with respect to the Tarim Basin, the maximum left-lateral displacement on the Altyn Tagh fault since 24 Ma is 500 ± 130 km. *INDEX TERMS:* 1525 Geomagnetism and Paleomagnetism: Paleomagnetism applied to tectonics (regional, global); 1527 Geomagnetism and Paleomagnetism: Paleomagnetism applied to geologic processes; 8105 Tectonophysics: Continental margins and sedimentary basins; *KEYWORDS:* Altyn Tagh fault, paleomagnetism, central Asia, Qaidam, rotation, kinematics. **Citation:** Chen, Y., S. Gilder, N. Halim, J.-P. Cogné, and V. Courtillot, New paleomagnetic constraints on central Asian kinematics: Displacement along the Altyn Tagh fault and rotation of the Qaidam Basin, *Tectonics*, *21*(5), 1042, doi:10.1029/2001TC901030, 2002.

1. Introduction

[2] The world's most impressive example of active continent-continent collision occurs where India continues its northward propagation into the Asian landmass, some 50 million years after their initial contact. Deformation resulting from this collision has created an extensive network of strike-slip faults and high mountain ranges (Figure 1). To the south, near the ancient subduction zone, are the Himalaya Mountains. To their north lies the vast Tibetan plateau—a remarkably flat topographic feature spanning 3×10^6 km^2 and standing some 5 km above sea level. Tibet's northern margin is flanked by the >2000 km long EW trending Kunlun Mountains. North of these mountains are the Tarim and Qaidam basins which are in turn bordered to the north by the Tian Shan and Qilian mountains, respectively (Figure 1). Separating the Tarim and Qaidam basins is the ~1500 km long, N70°E trending Altyn Tagh fault. As the average elevation of these basins is about 1500 m and 3000 m, respectively, the Altyn Tagh fault forms a giant step with 1500 m of vertical offset.

[3] Just how and when these topographic and tectonic features formed is a subject of active research. A kinematic model of the velocity field of present-day deformation in central Asia was proposed by *Avouac and Tapponnier* [1993] (Figure 1a). Their model divides the region into distinct blocks that undergo finite rotations accommodated along major strike-slip faults which bound the blocks. This model is interesting because it can be tested from a paleomagnetic point of view: one can for instance estimate since when the present velocity field

[1]Département des Sciences de la Terre, ISTO, Université d'Orléans, Orléans, France.
[2]Laboratoire du Paléomagnétisme, Institut de Physique du Globe de Paris, Paris, France.
[3]Laboratory of Paleomagnetism, Kobe University, Japan.

0278-7407/02/2001TC901030

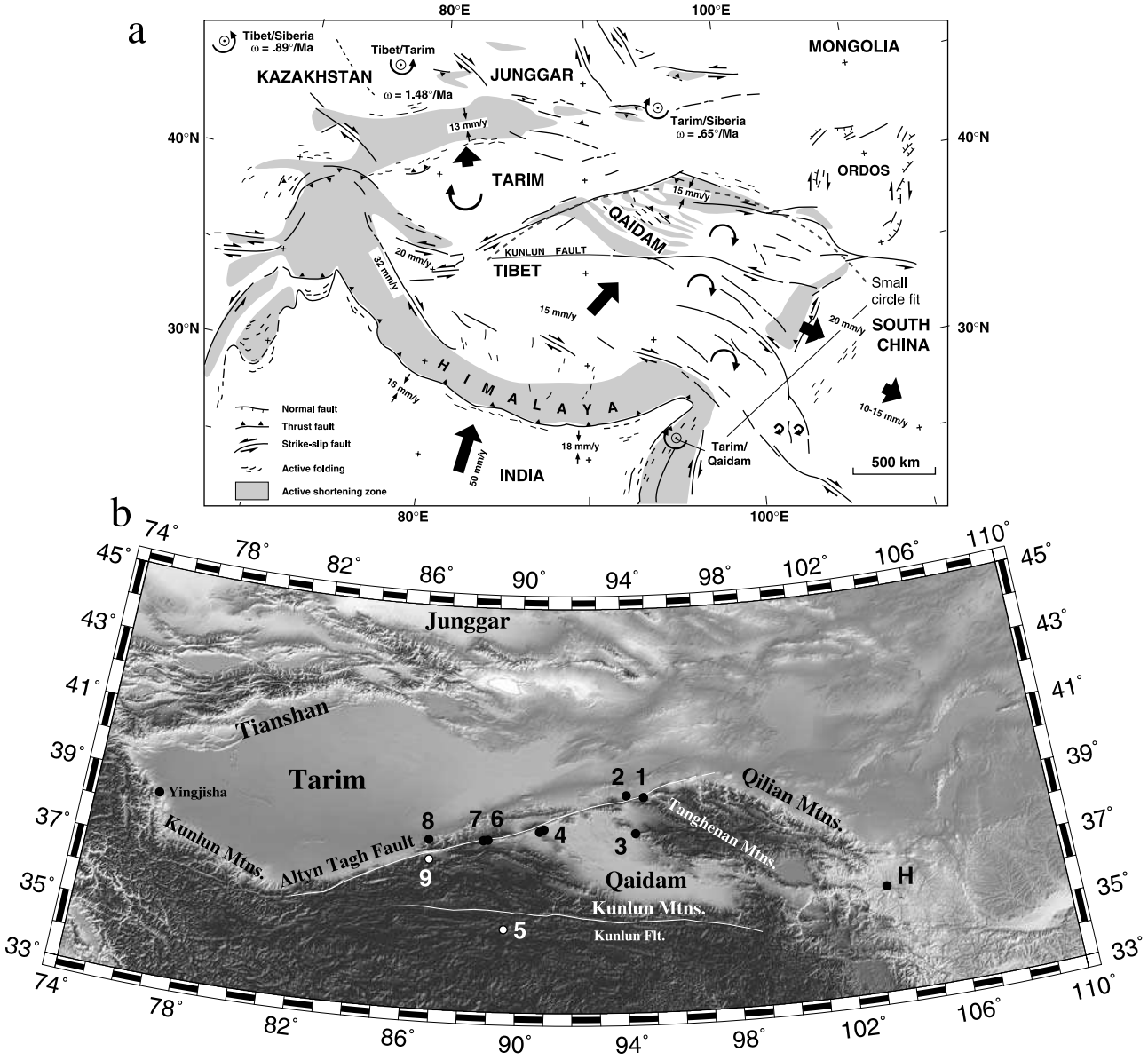

Figure 1. (a) Schematic tectonic map of central Asia [after *Avouac and Tapponnier*, 1993]; (b) Topographic map of sampling areas. Sampling locations from this study: 1, Subei; 2, Aksai; 3, Mahai; 4, Huatugou+Honggouzi+Xorkol; 5, Kekexili; 6, Bulabashi; 7, Valley; 8, Qiemo; 9, Tula. H is the sampling locality of *Halim et al.* [1998].

could have applied. Thus to better understand the long-term evolution of the central Asian theater, we collected paleomagnetic samples in and around the Altyn Tagh fault and surrounding basins. In particular, the Qaidam Basin has been considered a modern analog of how Tibet formed [*Tapponnier et al.*, 1990, 2001]. In this model, the mountains surrounding the basins grow faster than rivers can incise them, which leads to an internal drainage system. The basin's interior then becomes flooded with sediment eroded from the surrounding mountains. This process of margin growth and internal sedimentation contributes to a relatively high and flat plateau interspersed with mountains within the plateau's interior. In the Qaidam Basin these internal mountain ranges are bordered by thrust faults that trend obliquely to the Altyn Tagh fault. Mountain ranges are absent in the Tarim Basin, north of the Altyn Tagh fault, thus the fault must accommodate left-lateral motion to compensate for the differential crustal shortening between the Qaidam and Tarim basins [*Meyer et al.*, 1998].

[4] Most workers agree that the Altyn Tagh fault is a left-lateral strike-slip fault although the magnitude and time of motion is less clear [e.g., *Tapponnier et al.*, 1981; *Ritts and Biffi*, 2000]. Amount of offset varies from

60 to 700 km based on the proposed across fault correlation of offset geologic units; other work has focused on dating terraces or other offset geomorphologic features to constrain recent slip rates, then extrapolated those rates to the past (see discussion below). Paleomagnetic constraints on the amount of displacement along the Altyn Tagh fault are difficult to establish because the fault's easterly strike would require thousands of kilometers of offset in order to be resolvable by paleolatitude differences. One way around this problem is to use paleomagnetic rotations. First, if the Qaidam Basin rotated relative to the Tarim Basin, the relative motion must be mostly taken up by slip along the Altyn Tagh fault. Second, one can sample time-progressive sequences to determine when (or if) a particular block had (or had not) rotated. A paleomagnetic study along the Altyn Tagh fault by *Rumelhart et al.* [1999] argued that no significant offset occurred along the Altyn Tagh fault since the Oligocene; however, their interpretations were jaded by a miscalculation of the amplitude and sign of rotation [*Yin et al.*, 2000]. Changes in the rock magnetic record of Subei (near the eastern flank of the Altyn Tagh fault) suggest that the nearby Tanghenan Mountains uplifted rapidly at 23 to 21 Ma and that Subei rotated 27° ± 5° counterclockwise after 19 Ma [*Gilder et al.*, 2001]. In order to help elucidate the tectonic evolution of the Qaidam Basin and the Altyn Tagh fault under the influence of the India-Asian collision, we studied some 1500 paleomagnetic cores from the Qaidam and Tarim basins and from northern Tibet. The results from this study are reported below.

2. Mesozoic to Recent Geology and Paleomagnetic Sampling

[5] Sedimentary successions often crop out in the thrust packages exposed at the base of the mountains in central Asia. These, mainly Cenozoic, prograding sedimentary profiles are fairly monotonous throughout the region. The basal parts of the sequences are mainly fine-grained and represent deposition centers lying at some distance from the uplifting mountains. When crustal shortening and mountain building occurs, the mountains encroach upon the basins, which leads to progressively larger grain sizes reflecting increasingly proximal deposition. We have observed these coarsening-upward sedimentary sequences all around the margin of the Tarim Basin, on both sides of the Tian Shan and within the Qaidam Basin; however, they are not necessarily coeval, even within a few millions of years. This is why we think that age constraints solely based on facies correlation can have significant (10–20 Myr) errors. Pre-Cenozoic sediments are generally distinct from Cenozoic sediments and are fairly repetitive throughout central Asia. Cretaceous sediments are generally red to brick red, whereas Upper Jurassic red beds are interbedded with green sandstones and siltstones. Here again considerable overlap likely exists in time, which most probably leads to age uncertainties larger than those for the Cenozoic. Exceptions are in the western part of the Tarim Basin (and also in the Lhasa block) where fossiliferous Cretaceous and Paleogene marine carbonates crop out within the red bed sequences. Below we describe the sedimentary successions sampled from thirteen separate time/space localities in 1996 and 1997 (Figure 1).

2.1. Qaidam Basin

2.1.1. Huatugou Region–Jurassic (J_{3h}) and Cretaceous (K_{1q}) (Figure 1b, 4)

[6] A roughly 500 m thick section of alternating dark red to gray-green sandy mudstones and sandstones crops out northwest of Huatugou town. There, we collected nine sites in the red horizons of the Hongshuigou formation (Table 1 and Figure 2). Ostracods, *Cetacella hongshuigouensis*, *Darwinula paramagna* and *Sinoestheria tsaidamensis*, found in this section identify it as Upper Jurassic (J_{3h}) [*Bureau of Geology and Mineral Resources of Qinghai Province* (*BGMRQP*), 1991]. An unconformity separates them from the overlying Lower Cretaceous Quanyagou formation (K_{1q}), which is divided into two units. The upper unit is composed of brown to gray conglomerate and light red coarse sandstone while the lower one contains gray to white conglomerate and red sandstone. Ostracods such as *Darwinula sp.*, *Timiriasevia sp.* and *Lycopterocypris sp.* were identified in this section, whose thickness is about 130 m. Only five sites were drilled because of limited exposure and fairly constant bedding attitudes (Table 1).

2.1.2. Huatugou Region–Neogene (N) (Figure 1b, 4)

[7] Tertiary continental sediments in the Qaidam Basin reach several kilometers and serve as the main oil producing layers in the basin [*Ritts et al.*, 1999]. The Upper Neogene Youshashan and Shizigou formations are widespread in the Qaidam Basin, with a thickness of about 1500 m. These strata are mainly composed of yellow to light green mudstone and light to dark red sandstone and conglomerate. At the type section of Youshashan, as well as in our sites near Huatugou (Figure 2), charophyte and ostracod fossils such as *Charites molassica*, *Tectochara, sp.*, *Cyprinotus sp.*, *Eucipris sp*. were identified [*BGMRQP*, 1991]. These units conformably overlie the upper Lower Neogene (Upper Miocene), Upper Gancaigou formation (N_{1g}) [*BGMRQP*, 1991], whose age is constrained by Ostracods *Hemicyprinotus valvaetumitus*, *Patamocypris sp.*, and *Limnocythere sp.* Altogether, we sampled three sections of 24 Neogene sites in the vicinity of Huatugou, and another 10 sites at Honggouzi, about 50 km north of Huatugou. The 10 Honggouzi sites are mapped as the Upper Neogene Youshashan formation (N_{2y}). These sites, plus another nine (c625–c634) belonging to the Upper Neogene Shizigou formation (N_{2sh}), were sampled along the Huatugou–Xorkol road (section A in Table 1 and Figure 2). At two other sections, eight sites (c716–c723, N_{1g}) of light yellow-colored sandstone and six sites (c724–c729, N_{2sh}) of red muddy sandstone were sampled, respectively (sections B and C in Table 1 and Figure 2). The age of the most recent deformation is Quaternary, as evidenced by a marked angular unconformity clearly observed 6 km NW of Huatugou; however, another deformation phase

Table 1. Summary of Paleomagnetic Results From This Study[a]

Site	n/N	S/D	Dg	Ig	Ds	Is	k	α_{95}
			Qaidam					
Huatugou (Figure 1b, and 4), J3h, 38.46°N, 90.75°E								
c610	7/7	182/18	244.4	−23.9	238.7	−39.5	35.2	10.3
c611	6/7	199/15*	232.4	−29.4			18.9	15.8
					223.9	−33.5	19.9	15.4
c612	6/6	80/61.5	210.1	4.6	225.8	−39.1	19.9	12.5
c613	8/8	80/7	213.0	−34.0	216.6	−38.9	84.2	6.1
c614	8/8	35.5/14	221.3	−19.7	226.1	−17.7	57.1	6.8
c615	8/8	36/14	208.4	−41.8	221.1	−42.1	37.2	9.2
c616	8/8	84/21.5	212.5	−18.6	219.8	−34.7	29.9	10.3
c617	6/6	321/32*	177.4	−56.9			17.0	16.7
					197.1	−33.3	18.1	16.2
c622	8/8	315/54	166.9	−80.3	215.6	−30.5	70.1	6.7
Average	**9/9**		**36.0**	**34.3**			**8.1**	**19.2**
					40.4	**34.8**	**48.5**	**7.5**
Huatugou (Figure 1b, and 4), K1q, 38.44°N, 90.73°E								
c618	7/8	80/39	13.3	4.4	20.8	39.4	31.4	10.9
c619	7/8	79/39	15.0	6.7	24.0	40.7	12.8	17.5
c620	5/6	91.5/42	11.4	−5.9	13.6	35.2	17.3	18.9
c621	5/6	91.5/42	21.1	−8.0	24.4	31.2	51.5	10.7
c623	0/5	122/31						
Average	**4/4**		**15.2**	**−0.7**			**98.4**	**9.3**
					20.7	**36.7**	**188.0**	**6.7**
Huatugou (section A, Figures 1b, 4 and 2), N2sh, 38.35°N, 90.80°E								
c625	9/9	143/51	18.3	18.1	347.7	53.5	83.3	5.7
c626	7/8	153.5/61	202.3	−.2	182.3	−41.2	29.5	11.3
c627	8/8	152/62	210.0	−14.5	169.9	−57.2	97.7	5.6
c628	9/9	159/36.5	30.4	29.5	4.1	53.3	35.1	8.8
c629	8/9	227.5/9	186.5	−60.2	176.8	−53.7	25.0	11.3
c630	13/13	226/10.5	195.5	−56.5	184.1	−50.3	138.9	3.5
c631	7/12	207/8.5	203.5	−52.3	192.9	−51.0	74.1	7.1
c632	7/11	204.5/13.5	203.7	−53.9	185.9	−51.6	44.4	9.2
c634	5/9	273/17.5	357.3	61.3	359.1	44.1	17.5	18.8
Average	**9/9**		**20.6**	**39.1**			**11.3**	**16.0**
					0.6	**50.9**	**134.5**	**4.5**
Huatugou (section B, Figures 1b, 4 and 2), N1g, 38.38°N, 90.90°E								
c716	0/5	80/14						
c717	0/6	106/15						
c718	0/6	124/21						
c719	0/6	117/26						
c720	8/8	113/49	186.0	4.3	179.9	−42.2	23.2	11.7
c721	8/9	114/50	.7	−4.6	352.8	40.6	11.4	17.1
c722	8/9	117/55	182.0	4.0	170.8	−44.5	31.8	10.0
c723	9/10	129/54	11.2	5.4	352.6	50.2	18.9	12.2
Average	**4/8**		**5.0**	**−1.9**			**143.5**	**7.7**
					354.1	**44.4**	**252.0**	**5.8**
Huatugou (section C, Figures 1b, 4 and 2), N2sh, 38.27°N, 90.92°E								
c724	8/8	325.5/7.5	348.3	42.1	354.1	38.9	25.7	11.1
c725	9/9	10/17*	351.3	45.3			99.7	5.2
					11.7	47.8	90.6	5.4
c726	8/9	352.5/20	350.7	44.5	9.6	41.8	93.2	5.8
c727	8/8	136/31	11.7	25.0	355.7	48.4	74.6	6.5
c728	7/9	137/34.5	13.5	16.6	.2	43.5	13.1	17.7
c729	8/9	118/76	174.9	33.6	175.2	−32.9	37.0	9.2
Average	**6/6**		**359.5**	**25.1**			**6.9**	**27.5**
	6/6				**0.8**	**42.4**	**100.0**	**6.7**
Huatugou overall average	**19/24**		**9.9**	**26.1**			**7.8**	**12.9**
					359.2	**46.9**	**102.9**	**3.3**
Honggouzi (Figure 1b,4), N2y, 38.68°N, 91.10°E								
c636	10/12	160/49	35.7	32.4	345.9	61.6	77.4	5.5
c637	6/8	160/49	26.6	22.9	352.7	49.7	41.7	10.5
c638	11/11	333.5/26.5	152.5	−62.2	193.1	−52.6	71.0	5.5

Table 1. (continued)

Site	n/N	S/D	Dg	Ig	Ds	Is	k	α_{95}
c639	4/4	336/34.5	129.5	−65.5	200.5	−58.5	44.8	13.9
c710-2	7/7	267/18	8.9	67.3	4.1	49.6	38.9	9.8
c711	6/7	266.5/18	8.2	67.0	3.6	49.2	46.4	9.9
c712	6/6	235/18*	195.7	−71.7			26.8	13.2
					182.3	−56.1	35.1	11.5
c713	6/6	290/30	142.3	−76.9	182.1	−51.5	116.3	6.2
c714	6/6	287.5/28	287.9	78.5	354.0	59.8	95.1	6.9
c715	6/6	313/28	129.5	−62.4	173.3	−52.8	227.4	4.5
Average	**10/10**		**358.2**	**65.6**			**10.9**	**15.3**
					1.3	**54.5**	**122.2**	**4.4**
Mahai (Figure 1b, 3), E3g, 38.4°N, 94.3°E								
c642	9/9	117/86*	211.2	46.9			41.5	8.1
					210.5	−37.4	62.9	6.5
c643	5/5	112/76	195.6	46.4	196.9	−29.4	12.0	23.1
c644	6/8	305/52.5	141.7	−85.4	209.4	−36.0	12.5	19.7
c645	9/9	316/37.5	140.6	−64.0	188.6	−43.9	25.1	10.5
c646	5/7	51/29*	184.3	−31.2			39.0	12.4
					205.0	−53.7	23.5	16.1
c647	9/13	105.5/65	201.0	14.3	204.0	−50.4	102.1	5.1
c648	4/6	316.5/79	51.3	−75.9	225.1	−25.3	16.2	24.9
Average	**7/7**		**7.6**	**27.1**			**1.8**	**65.2**
					26.2	**40.0**	**34.1**	**10.5**
Subei (Figure 1b, 1), E3-N1, 39.5°N, 94.7°E								
Magneto-stratigraphy	222/373	98/48*	355.1	−2.2	350.2	43.8	12.9	2.7
c601	4/6	282/71	47.5	−46.8	153.8	−49.8	16.2	23.6
c602	4/7	274/90	177.8	54.8	179.6	−35.0	415.3	4.8
c603	4/6	265/61	0.9	−63.7	170.3	−55.1	19.6	22.5
Average	**4/4**		**198.4**	**31.0**			**1.3**	–
					349.0	**46.4**	**50.6**	**13.0**
Xorkol (Figure 1b, 4), J2, 38.65°N, 91.30°E								
Hand	5/8			34.0			14.6	20.7
samples						17.8	71.4	9.1
Bulabashi coal mine (Figure 1b, 6), J1-2, 38.12°N, 88.82°E								
c734	6/10	84.5/65	13.2	48.5	147.2	62.2	50.3	9.7
c735	7/9	87/45*	9.6	66.1			36.8	10.1
					160.9	69.8	14.9	16.2
c736	9/9	91.5/77	358.9	59.1	183.6	43.8	247.8	3.3
c737	8/8	90/63	13.0	61.7	169.8	54.3	46.5	7.6
Average	**4/4**		**9.1**	**59.0**			**97.3**	**9.4**
					168.0	**58.3**	**34.0**	**16.0**
Bulabashi coal mine (Figure 1b, 6), J3, 38.15°N, 88.82°E								
c730	6/10	287/6/66						
c731a	6/9	284/50						
c731	3/7	163.5/21						
c732	0/10	162/2						
c733	3/8	48/55						
Average	**18/44s**		**319.6**	**46.5**			**6.6**	**14.7**
					339.1	**30.8**	**45.9**	**5.4**
Valley west of Balabushi coal mine (Figure 1b, 7), N, 38.16°N, 88.70°E								
c738	7/8	247/37	20.0	74.2	351.2	40.4	7.8	24.8
c739	7/9	112/87	167.3	47.6	175.4	−31.0	11.6	19.6
c740	5/8	110.5/80	200.3	40.8	200.3	−39.2	14.7	21.2
Average	**3/3**		**7.3**	**−14.7**			**1.5**	**
					2.1	**37.6**	**36.6**	**20.7**
Tula (Figure 1b, 9), E-K, 37.59°N, 86.71°E								
c741	0/8	78/45						
c742	7/9	89.5/53	187.0	−4.8	193.3	−57.1	21.8	13.2
c743	4/7	88/29	27.0	11.5	34.1	36.1	19.5	21.4
c744	3/6	78/45	166.4	10.1	166.0	−34.9	32.7	21.9
c745	0/6	112/53						
c746	0/6	115/57						
c747	5/8	107/107	316.6	77.6	207.9	−10.6	31.8	13.8

Table 1. (continued)

Site	n/N	S/D	Dg	Ig	Ds	Is	k	α_{95}
c748	6/8	285/20	46.3	55.0	37.0	37.0	26.4	13.3
c749	4/5	280/18	51.7	60.6	37.9	45.6	24.7	18.9
Average	**6/9**		**20.9**	**12.9**			**2.2**	**60.9**
					23.4	**38.4**	**13.7**	**18.8**
				Tibet				
Kekexili (Figure 1b:5), N1ch, 36.05°N, 89.27°E								
c703	3/9	355.5/25.5	335.7	25.3	5.6	35.3	108.8	11.9
c704	8/8	358.5/12	349.4	58.6	41.0	52.3	20.5	12.5
c705	8/9	73.5/33	9.2	30.7	42.9	51.0	12.6	16.3
c706	8/15	78/38*	355.6	6.5			11.9	17.1
					4.4	49.0	12.4	16.8
c707	6/15	93/45	350.8	2.4			85.2	7.3
					347.0	53.2	84.3	7.3
c708	8/11	8.5/25	341.7	34.5	20.9	41.6	9.9	19.5
c709	5/12	13/31*	341.5	37.5			11.3	23.8
					30.2	43.3	12.5	22.5
c710	9/9	313/46	299.4	62.3	32.3	38.5	24.9	10.5
Average	**8/8**		**346.0**	**33.3**			**10.1**	**18.3**
					20.7	**47.0**	**30.2**	**10.2**
				Tarim				
Aksai (Figure 1b, 2), E3b, 39.2°N, 94.3°E								
c604	12/12	138/42	211.5	4.5	207.6	−35.5	21.6	9.6
c605	9/11	138/42	205.9	−2.2	198.5	−40.4	34.2	8.9
c606	4/4	319/26	174.9	−44.0	188.6	−26.1	46.1	13.7
c607	12/13	338.5/31	9.1	64.8	39.2	41.6	31.2	7.9
c608	8/12	337/25	341.5	57.1	12.9	48.0	29.7	10.3
c609	8/12	322.5/50	150.5	−70.6	208.8	−34.8	38.1	9.1
Average	**6/6**		**9.6**	**41.8**			**5.1**	**32.9**
	6/6				**22.5**	**38.2**	**48.7**	**9.7**
Qiemo (Figure 1b, 8), E-N, 38.10°N, 86.57°E								
c750	7/14	48/17*	178.9	−31.6			13.0	17.4
					185.9	−42.5	15.0	16.1
c751	0/9	70/24.5						
c752	0/7	70/24.5						
c753	6/9	225/85	102.7	32.3	358.9	49.3	65.7	8.3
c754	5/7	225/85	273.5	−27.6	190.5	−44.6	32.8	13.6
c755	6/8	225/85	97.3	35.3	358.8	43.9	11.3	20.9
c756	8/8	227/85	270.1	−27.2	195.3	−40.1	17.9	13.5
c757	5/8	227/85	282.0	−35.5	179.1	−45.6	23.1	16.3
c758	6/8	227/85	268.5	−10.3	217.8	−41.6	29.7	12.5
Average	**7/9**		**86.0**	**32.6**			**7.1**	**24.3**
					9.7	**44.7**	**59.3**	**7.9**

[a] Abbreviations are n/N, number of samples used to calculate mean direction/number of samples demagnetized; *D*, declination; *I*, inclination; *g*, in situ (geographic) coordinates; *s*, tilt-corrected (stratigraphic) coordinates (at 100% unfolding); α_{95}, the radius that the mean direction lies within 95% confidence; *k*, the best estimate of the precision parameter; S, strike = dip direction of beds - 90°; N_2, Upper Neogene (Plio-Pleistocene); N_1, Lower Neogene (Miocene); E_3, Oligocene; E1, Paleocene; K_1, Lower Cretaceous; J_3, Upper Jurassic; *mean value; **s**, specimen mean; J3h, Upper Jurassic Hongshuigou formation; K1q, Lower Creaceous Quanyagou formation; N1g, Lower Neogene Ganchaigou formation; N2sh, Upper Neogene Shizigou formation; N2y, Upper Neogene Yousahshan formation; E3g, Upper Eocene Gachaigou formation; N1ch, Lower Neogene Chabaoma formation; and E3b, Upper Eocene Baiyang formation.

occurred sometime between the Upper Jurassic and Neogene (Figure 2).

2.1.3. Xorkol (J_2) (Figure 1b, 4)

[8] Northeast of Huatugou, just southeast of Xorkol near the Altyn Tagh fault (Figure 1), eight large block samples were taken from a strongly deformed fine red sandstone. Each block sample had a unique bedding attitude that was collected from a fold with a steeply plunging axis. The age is constrained as Middle Jurassic based on the palynology dominated by the assemblage of *Corollina sp.*, *C. meyerana*, *Classopollis annulatus* and *Duplexisporites sp*. [*Ritts and Biffi*, 2000].

2.1.4. Mahai (E_{1-2l} to E_{3g}) (Figure 1b, 3)

[9] Well within the interior of the Qaidam Basin, about 100 km northwest of Daqaidam town, a strongly folded and faulted sedimentary section is exposed. The base of the section contains the Lower Cretaceous Quanyagou formation (K_{1q}). Above this is a series of red siltstone and red fine to coarse sandstone, called the Lulehe (E_{1-2l}) and Lower Gachaigou (E_{3g}) formations, which are dated by ostracods,

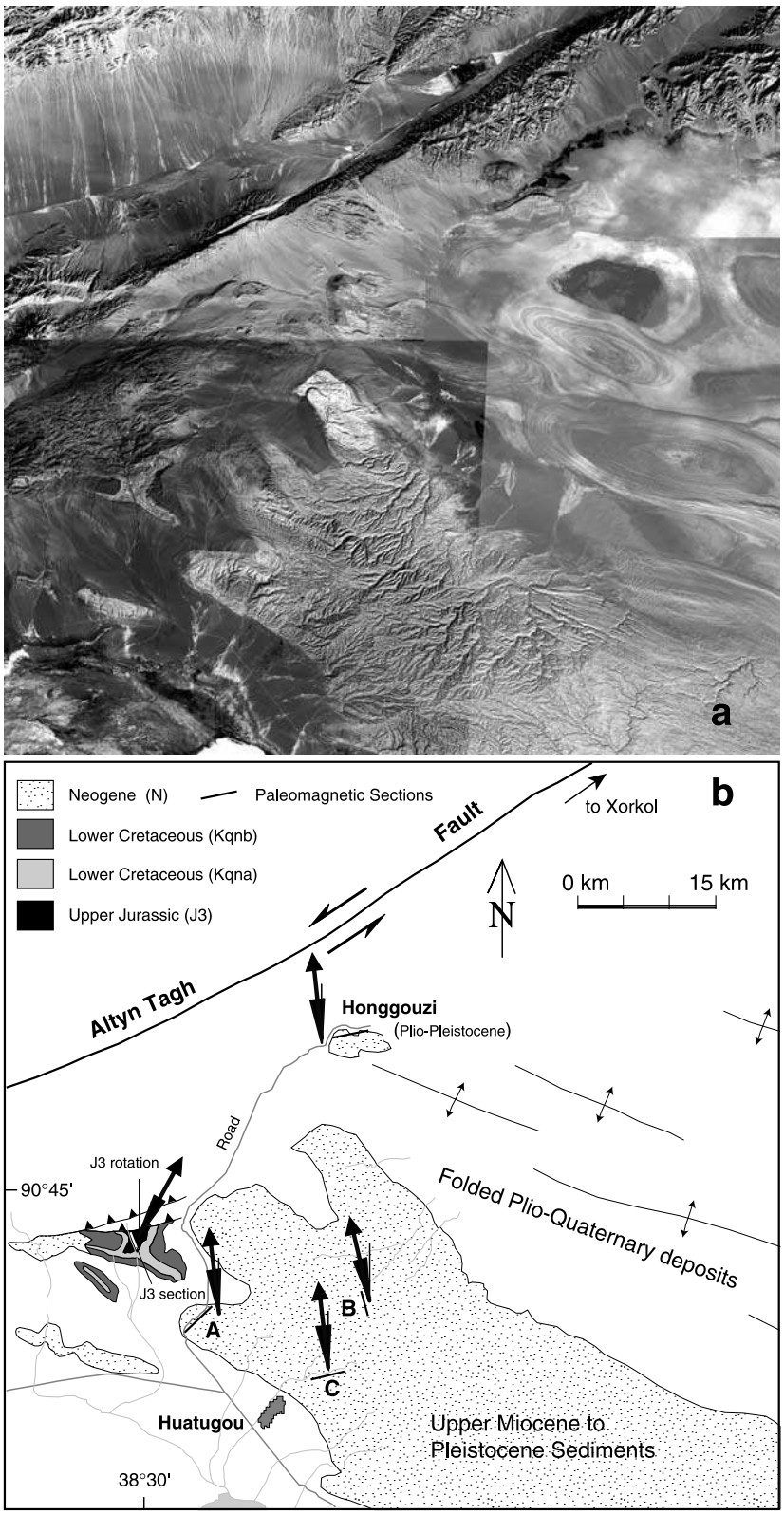

Figure 2. Spot image (a) and simplified geologic map (b) (after unpublished local geological brigade map 1:200,000 and field notes) of the Huatugou area. Paleomagnetic rotations and error cones from Tables 1 and 2. A, B, and C represent the three Neogene sections sampled in this area, with corresponding sampling sites, as well as those from the Honggouzi Upper Neogene sediments and the Upper Jurassic red beds, listed in Tables 1 and 2.

Ilyocypris sp., *Cyclocypris sp.*, *Candona sp.*, and *Kassininaclinocauda*, charophytes, *Obusochara brevicylindrica* and *Gyrogona sp.*, and gastropods such as *Hydrobia sp.* We could not distinguish the two formations (E_{1-2l} and E_{3g}), from which we sampled seven sites (c642–c648; Table 1 and Figure 1). This Paleogene series is in fault contact with overlying N_{1g} red beds.

2.1.5. Subei (E_3–N_1) (Figure 1b, 1)

[10] The detailed magnetostratigraphy of the Xishuigou section, Subei is described by *Gilder et al.* [2001]. The polarity succession together with Late Oligocene (E_3) to Early Miocene (N_1) mammal and charophyte paleontology dates the succession as 26.1 Ma to 18.8 Ma. The sediments coarsen from bottom to top. The base consists of poorly indurated brick red mudstone, claystone and siltstone. Dominating the uppermost part of the section are 3 to 10 m thick conglomerate beds, intercalated with small sandy lenses, that have well rounded to slightly angular clasts measuring up to 1 m in diameter. We collected 538 paleomagnetic samples along a well-exposed, 2907 m long section for magnetostratigraphy and another three sites with different bedding attitudes in order to have a significant application of the fold test (Table 1).

2.1.6. Balabushi Coal Mine (J_{1-2y} and J_{3k}) (Figure 1b, 7)

[11] Balabushi Coal mine is located close to the Altyn Tagh fault (Figure 1b, 7) where strongly deformed Mesozoic rocks unconformably overlie Proterozoic basement. We sampled four sites in the Lower to Middle Jurassic Yerqiang formation (J_{1-2y}), which are made up of green to gray sandstone. Plant and gastropod fossils identified in this formation include *Conipteris hymenophylloides*, *Otoramites bengalensis* and *Probachia sp.* [*Bureau of Geolology and Mineral Resources of Xinjiang Uygur Autonomous Region* (*BGMRXUAR*), 1993]. These beds are unconformably overlain by the Upper Jurassic Kuzigongsu formation (J_{3k}), from which we sampled five sites of red medium to fine grained sandstones. The Upper Jurassic age was taken at face value from the map [*BGMRXUAR*, 1993]; we know of no direct fossil control.

2.1.7. Valley South of Bulabashi (N) (Figure 1b, 6)

[12] A succession of more than 2500 m of Tertiary sediments is located south of the Balabushi Coal mine on the southern flank of the Altun Shan. In one terraced valley, we drilled three sites of soft, red, clay-rich sandstone and siltstone intercalated with gypsum. These lithologies are described as lower Upper Neogene by *Chen et al.* [1985] and as the Miocene (Lower Neogene) Shibiling formation (N_{1s}) by *BGMRXUAR* [1993]. The latter provides a list of ostracod fossils such as *Limnocyhere cinctura* and *Ilyocypris sp.*

2.1.8. Tula (K-E?, E_3?) (Figure 1b, 9)

[13] A series of Mesozoic to Cenozoic continental deposits with E-W trending fold axes are exposed south of Tula village (Figure 1) where we drilled nine red sandstone and siltstone sites. The series varies in thickness from 230 to 1700 m. Its age is believed to be Cretaceous to Eocene by *Chen et al.* [1985] and Oligocene by *BGMRXUAR* [1993] based on ostracod fossils such as *Cyprinotus sp.*, *Cypris sp.* and *Eucypris sp. Lockley et al.* [1999] reported fossilized tridactyl vertebrate tracks from Tula and placed them within the Paleogene based on correlation with similar tracks from other continents.

2.2. Tibet

[14] Kekexili (N_{1ch}) (Figure 1b, 5) lies in an extremely remote area of the Tibetan plateau, south of the left-lateral Kunlun fault (Figure 1b, 5). A more than 1000 m thick succession of red sandstone, conglomerate and numerous volcanic flows, dated (method unknown) between 10 Ma and 24.6 Ma [*BGMRQP*, 1991] crops out in several discrete basins. We sampled eight sites of red sandstone across a slightly plunging fold. No fossils are described for the red beds we sampled, but some late Miocene to Pliocene fossils, such as *Cyprinotus*, *cf. mancus*, *Eucypris sp.* and *Condoniella sp.*, were identified in the overlying deposits [*BGMRQP*, 1991]. Correlated with, but to the south of our section, are red beds intercalated with Lower Miocene volcanic rocks that are assigned to the Chabaoma group (N_{1ch}) [*BGMRQP*, 1991].

2.3. Tarim Basin

2.3.1. Aksai (E_{3b}) (Figure 1b, 2)

[15] We drilled 64 cores at six sites from two fold limbs in the lower part of a section in the Hongliugou Valley, north of the Altyn Tagh mountains, on the southern margin of the Tarim Basin (Figure 1). There, more than 1000 m of Tertiary sediments unconformably overlie Early Proterozoic basement. No fossils are described for the sampled yellow to red siltstones. An Oligocene age was ascribed by stratigraphic correlation with the Baiyang formation (E_{3b}) from the Yumen Basin [*Bureau of Geolology and Mineral Resources of Gansu Province* (*BGMRGP*), 1989]. *Wang* [1997] correlated this section with the lower part of the Subei section (E_3). Mio-Pliocene, light red to yellow conglomeratic sandstone and muddy sandstone conformably overlie the beds we sampled thus giving a minimum age [*BGMRGP*, 1989].

2.3.2. Qiemo (E–N) (Figure 1b, 8)

[16] Southeast of Qiemo town, Mesozoic and Cenozoic sediments are exposed along the northern Altyn Tagh range near the southeastern border of the Tarim Basin (Figure 1). At Jianglesai village we collected nine sites in a thick, well-exposed section mapped as Paleogene to Neogene [*BGMRXUAR*, 1993], to which *Rumelhart et al.* [1999] assigned a mean age of 20 Ma. Steeply northward dipping beds (~85°) are exposed over 1 km, coarsening upward reminiscent of the Subei, Xishuigou section. Three sites were sampled in gently ESE dipping beds in the southernmost part of the section to provide a fold test.

3. Laboratory Treatment and Paleomagnetic Results

[17] Oriented blocks were collected from two sections (Xorkol and part of Mahai), but all other sites were sampled with a gasoline-powered drill. The cores were

oriented with magnetic and solar (whenever possible) compasses. Differences between the 1990 IGRF and the solar compass declinations proved almost always less than 3°. About eight cores were sampled per site, with one to two cores collected per bed. Each site normally comprises 10 to 15 m of stratigraphic thickness in order to average out geomagnetic secular variation. Classic stepwise thermal treatment with an average of about 15 steps was applied to one 2.5 cm by 2.2 cm specimen sliced from each core drilled in the field. Magnetic susceptibility was measured after each temperature step to track potential changes in the magnetic mineralogy. None was observed for the majority of the measured specimens. Stepwise AF demagnetization was applied to a few specimens per site. Magnetic vectors were measured on AGICO JR5-spinner and 2G 3-axis DC-SQUID magnetometers at the Université d'Orléans and at the Institut de Physique du Globe de Paris, respectively. Demagnetization data were analyzed using principal component analysis [*Kirschvink*, 1980] and *Fisher* [1953] statistics using computer programs written by R. Enkin and J. P. Cogné. Fold and reversal tests follow *McElhinny* [1964] and *McFadden and McElhinny* [1990], respectively, and were applied in all cases at the 95% confidence level.

[18] For each locality/age group, we systematically measured the acquisition of isothermal remanent magnetization (IRM) with an ASC Scientific IM10 pulse magnetizer and determined Curie temperatures with a AGICO CS3 furnace. Unless otherwise stated, these experiments indicate that the studied rocks contain both magnetite and hematite. In nearly all cases, thermal demagnetization isolates both low and high temperature components. As a whole, the low temperature component (LTC) (<300°C) in situ directions are close to the present Earth's field direction and fail the fold test. This component clearly represents a recent, post folding magnetization. Below we describe the directions isolated from the high temperature components (HTC) only.

3.1. Qaidam Basin

3.1.1. Huatugou Region: Upper Jurassic (J_{3h}), Lower Cretaceous (K_{1q}) and Neogene (N_{1g}=N_{2sh}) (Figure 1b, 4)

[19] The nine sites from the J_{3h} Hongshuigou formation yield magnetic directions of reversed polarity at high temperatures (Figure 3a). The site mean directions are better grouped in tilt-corrected than in situ coordinates and pass the fold test (Table 1 and Figure 4a; see also *Halim et al.* [2001]). All Lower Cretaceous (K_{1q}) samples show NE and down magnetic directions (Figure 3b), except for site c623 whose magnetic remanence was unstable. Site mean directions are somewhat better grouped after bedding correction than before, yet yield an inconclusive fold test due to nearly uniform bedding for the four sites (Table 1 and Figure 4b). The three Neogene sections have both normal and reverse polarities. Well-defined HTCs were isolated in nearly all measured specimens (Figure 3c), except for four sites whose directions became random above 500°C. The 19 site mean directions clearly group better after bedding correction with a positive fold test (Table 1 and Figure 4c); the mean directions for each one of the three sections calculated independently are indistinguishable at 95% confidence limits.

3.1.2. Huatugou Region- Honggouzi (N_{2sh}) (Figure 1b, 4)

[20] AF demagnetization removed more than 90% of the remanence (Figure 3d), yielding a well-defined magnetic component in the 10 to 150 mT range. Thermal demagnetization, which was applied to most specimens, isolated a stable component from about 200°C to 690°C (Figure 3e). Magnetic directions were the same regardless of the cleaning technique employed. Normal and reverse polarities are equally represented in the sample population (Figures 3d and 3e; Table 1). Both the fold and reversal tests are positive (Figure 4d and Table 1).

3.1.3. Xorkol (J_2) (Figure 1b, 4)

[21] IRM measurements show the presence of a hard coercivity magnetic mineral. Thermal demagnetization isolates two components in most specimens: one from room temperature to about 540°C and another from about 560 to 695°C (Figures 3h and 3i). The LTC directions are well grouped in geographic coordinates and lie close to the present field direction; however, this is not the case for the HTC directions. Core specimens drilled in the laboratory from five of the eight oriented block samples show well-defined trajectories. The mean inclinations for these five blocks become more coherent after bedding correction, with ks/kg = 5. However, the declinations are too dispersed to compute a mean direction, even after accounting for the steeply plunging fold axis (Figure 4f and Table 1). This may indicate that the area has suffered severe small-scale vertical-axis rotations or internal shearing.

3.1.4. Mahai (E1-2l to E_{3g}) (Figure 1b, 3)

[22] Thermal demagnetization eliminates a LTC until ~350°C, whereafter the remanent magnetization decreases linearly to the origin with a considerable intensity drop from 580 to 700°C (Figure 3f). Most tilt-corrected directions have upward inclinations and SW declinations. The site mean directions are much more tightly clustered after bedding correction and pass the fold test (Figure 4e and Table 1).

3.1.5. Subei (E_3-N_1) (Figure 1b, 1)

[23] The magnetization characteristics of the Subei rocks were discussed in detail by *Gilder et al.* [2001]. Thermal demagnetization shows a HTC that persists to 680°C (Figure 3g). 14 normal and 14 reverse magnetic chrons were identified in the section. The reversal test is negative, primarily because of differences in inclination and the small error ellipses that encompass the mean directions. The mean reverse polarity inclination is 8° shallower than for the normal polarity. This difference is most likely due to an incompletely removed overprint which, due to the folding geometry and the present magnetic field direction, steepens the normal polarity directions and shallows the reversed polarity directions. We also studied three sites about 1 km to the north in steeply dipping fine-grained sediments that correlate with the lower part of the magnetostratigraphic section. Treating the magnetostratigraphic section as one site, the fold test based on the four sites is clearly positive as

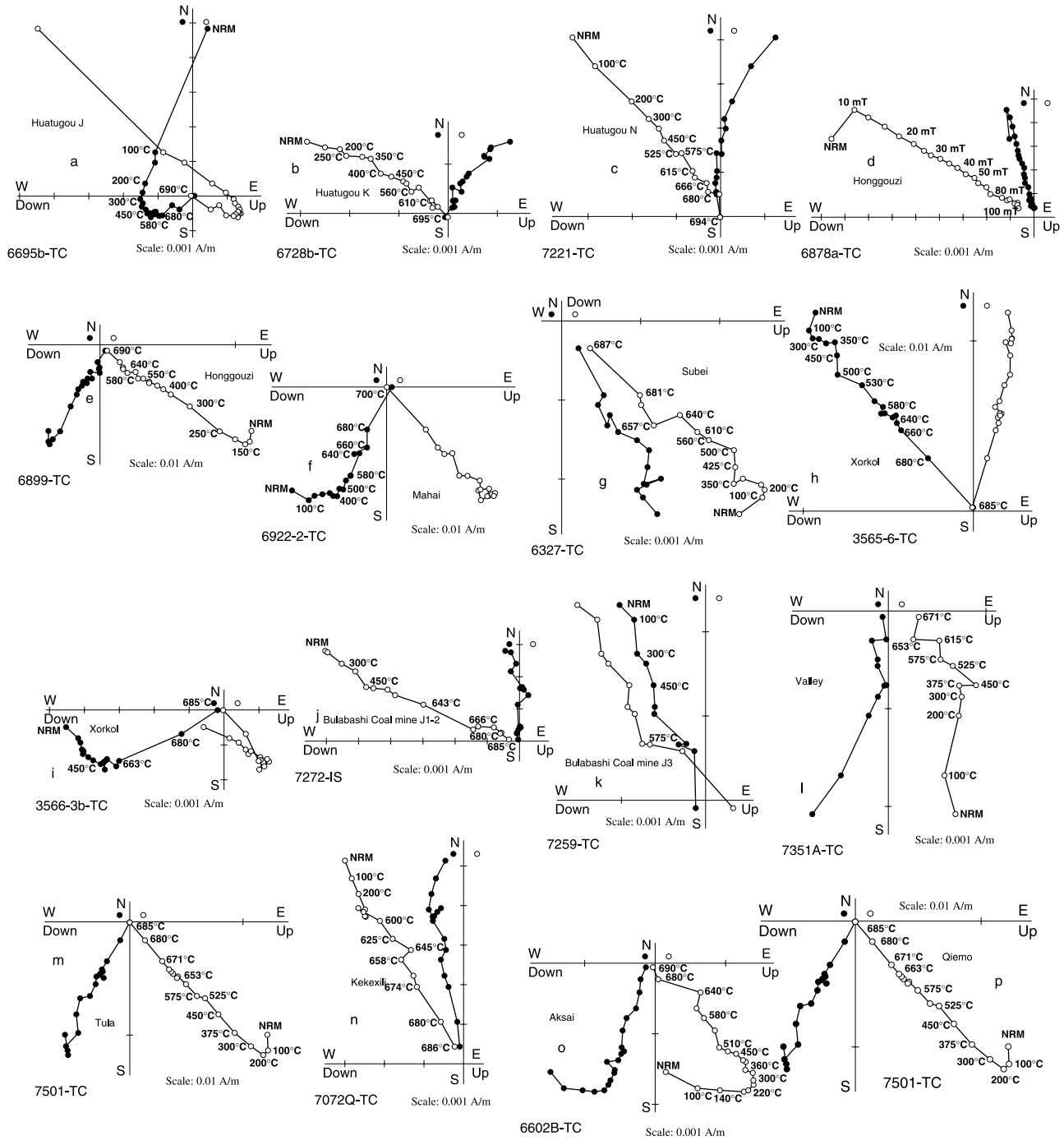

Figure 3. Orthogonal vector plots of representative specimens from each sampled age/locality group. Closed (open) symbols present the projection in horizontal (vertical) plane in stratigraphic coordinates (except 3j).

the precision parameter increases 39 times from in situ to tilt-corrected coordinates (Table 1).

[24] *Gilder et al.* [2001] found that a bedding parallel fault cuts the middle of the magnetostratigraphic section and argued from remanence data that the upper half was back (or clockwise) rotated about 15° with respect to the lower one. The AMS measurements on 262 samples support this observation as the maximum axis directions are also rotated about 15° across the fault. *Gilder et al.* [2001] considered that the mean tilt-corrected paleomagnetic direction from the footwall was more representative for the Subei section (D = 341.5°, I = 43.4°, n = 95 specimens, α_{95} = 4.0°) than the overall mean result. Both this direction and the overall mean direction are very similar to that found by *Rumelhart et al.* [1999] for Subei (D = 344.7°, I = 39.7°, α_{95} = 6.6°) from a somewhat smaller data set (n = 50).

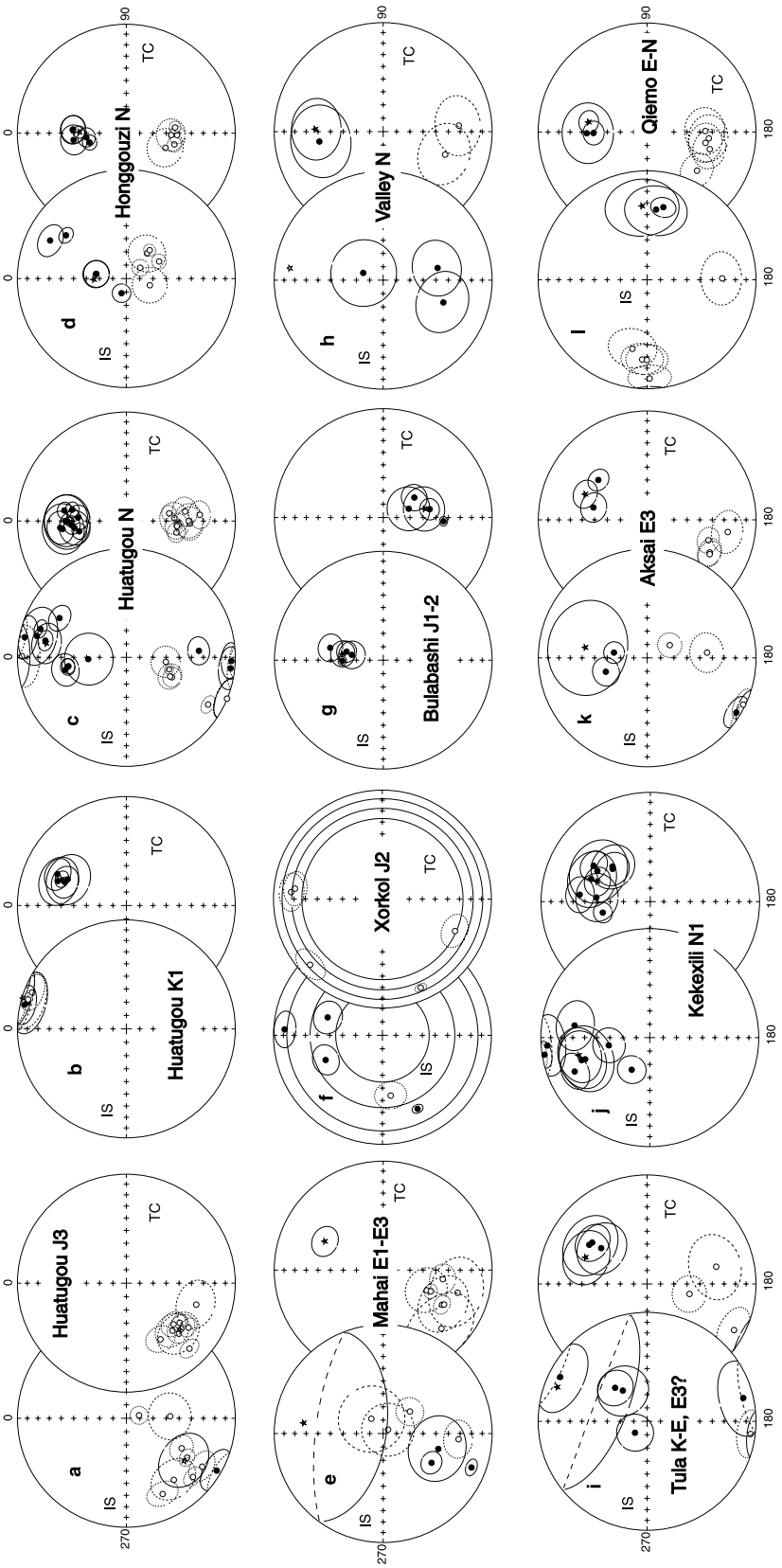

Figure 4. Equal-area stereonet plots of site mean directions (data from Table 1). Closed (open) symbols present downward (upward) magnetic directions. IS (TC) stands for in situ/geographic (tilt-corrected/ stratigraphic) coordinates.

3.1.6. Bulabashi Coal mine (J_{1-2y} and J_{3k}) (Figure 1b, 6)

[25] The four sites of vertically dipping, Lower to Middle Jurassic (J_{1-2y}) green sandstones show one north and down directed (in situ) magnetic component isolated from the initial NRM step to 685°C (Figure 3j). Well-grouped mean directions, with high k and low α_{95} values, are observed for each site (Table 1). The clustering of the site mean directions decreases, however, after bedding correction, indicating failure of the fold test. This, and the proximity of the overall mean direction to the present geomagnetic field direction suggests that these rocks were overprinted in the recent local field (Figure 4g and Table 1).

[26] The Upper Jurassic (J_{3k}) red sandstones mainly show unstable behavior during thermal demagnetization; magnetic directions could be interpreted for only 18 out of 44 specimens. Few of the 18 specimens show coherent directions at high temperatures (Figure 3k), so the great circle technique was applied to compute the mean direction [*Halls*, 1978; *McFadden and McElhinny*, 1988]. The precision parameter for the 18 samples increases sevenfold upon unfolding and the sample-level fold test is positive (Table 1).

3.1.7. Valley West of Bulabashi (N) (Figure 1b, 7)

[27] Thermal demagnetization reveals a dominant viscous component in most samples with some possessing linear demagnetization trajectories at high temperatures (Figure 3l). After heating to 300°C, the intensity generally becomes weak (about 10^{-4} A/m) and the appearance of the Zijderveld plots more erratic [*Zijderveld*, 1967]. The HTC directions are rather dispersed within each site with low k and high α_{95} values (Table 1). Both normal and reverse polarities are present and pass the reversal test. The site mean directions become more clustered after bedding correction, but the overall mean α_{95} value is large because of the considerable dispersion of the three individual site mean directions (Figure 4h and Table 1). Despite this, we tentatively regard the magnetization as primary because of the positive reversal test and because k increases 25 times upon unfolding.

3.1.8. Tula (K–E?, E_3?) (Figure 1b, 9)

[28] The high temperature component of the strongly folded (three overturned sites), red-green sandstones is fully unblocked at ~685°C (Figure 3m). Samples from three of the nine sites show only viscous magnetizations and were not considered further. The remaining six sites contain both polarities and pass the reversal test, but mainly because of the large uncertainty of the mean on the reverse polarity sites. The large dispersion of the reverse sites probably arises from a stronger contamination of the HTC by the LTC in comparison to the normal polarity sites. Site mean directions are better grouped after bedding correction with ks/kg = 6.2 and pass the fold test (Figure 4i and Table 1).

3.2. Tibet (Kekexili, N_{1ch}) (Figure 1b, 5)

[29] Magnetic mineralogy experiments on the red sandstones show that hematite carries the magnetic remanence because no Curie point less than 600°C is identified and the HTC unblocking temperature is ~680°C (Figure 3n). The majority of the samples show noisy thermal demagnetization behavior although some samples have well defined components that decay univectorally to the origin (Figure 3n). The HTC is of normal polarity only. As mentioned above, the sites were drilled across a plunging syncline (trending N99.6°E, 21°E) so a two-step unfolding procedure was applied to calculate the overall mean direction. The precision parameter of the site mean directions increases more than three times yielding a positive fold test (Figure 4j and Table 1).

3.3. Tarim Basin

3.3.1. Aksai (E_{3b}) (Figure 1b, 2)

[30] After removal of the LTC, an HTC was unblocked from about 350 to 680°C, showing a coherent direction that decays to the origin (Figure 3o). The HTC is represented by both magnetic polarities and passes the reversal test. The fold test is also positive with a 10 times increase of k after bedding correction (Figure 4k and Table 1).

3.3.2. Qiemo (E-N)

[31] An HTC for these red sediments unblocks from about 500°C to 685°C (Figure 3p). No HTC was isolated in two sites (c751 and c752) so they were excluded from the overall mean computation. The other seven sites show high dispersion due to a persistent viscous component; six have $\alpha_{95} > 12°$ (Table 1). Despite the relatively noisy data, both the fold and reversal tests are positive (Figure 4l and Table 1). The bedding corrected direction (D = 9.7°, I = 44.7°, α_{95} = 7.9°) is indistinguishable at the 95% confidence level [*McFadden and Lowes*, 1981] from *Rumelhart et al.'s* [1999] result of D = 358.4°, I = 39.6°, and α_{95} = 6.7°.

4. Discussion

4.1. Summary of Paleomagnetic Results

[32] We arrive at the following conclusions from the paleomagnetic data presented above. (a) LTC magnetic directions lie close to the present Earth's field direction and fail the fold test, indicating that they represent a remagnetization in the recent geomagnetic field. (b) The Late Jurassic, Paleogene and Neogene mean directions from Qaidam (Huatugou, Honggouzi, Subei and Mahai) and the Paleogene or/and Neogene of the Tarim Basin (Aksai and Qiemo) pass fold and/or reversal tests at the 95% confidence level, indicating their remanent magnetizations are surely pre-folding and most likely primary. We consider that the overall mean directions defined by these results have sufficiently averaged out secular variation to represent the time-averaged field. (c) The Lower Cretaceous sites from Qaidam (Huatugou) have normal polarity directions only, consistent with acquisition during the Cretaceous Long Normal Polarity Superchron. The precision parameter of the four sites improves after bedding correction. The overall mean direction is different from the present Earth's field and may represent a primary magnetic remanence, but we consider this a preliminary result and attach no weight to it. (d) The Bulabashi J_{3k} result is derived essentially from remagnetization circles

Table 2. Paleomagnetic Poles From This Study Together With Calculated Expected Declinations and Rotations[a]

Block	Locality (Number on Figures 1 and 6)	Age	λ_l (°N)	φ_l (°E)	λ_p (°N)	φ_p (°E)	A_{95} (°)	Dec_{exp}(°) Tarim	Dec_{exp}(°) NCB	Dec_{exp}(°) Eurasia	Rotation (°) Tarim	Rotation (°) NCB	Rotation (°) Eurasia
Qaidam	Honggouzi (4)	N_{2y}	38.6	91.1	86.5	254.2	5.7		7.3 ± 8.8	4.6 ± 3.2		−6.1 ± .8.8	−3.4 ± 6.2
	Huatugou (4)	N_{1g}-N_{2sh}	38.3	90.9	79.9	274.5	3.2		7.3 ± 8.8	4.6 ± 3.2		−7.5 ± 7.4	−5.3 ± 3.9
	Valley (7)	N	38.2	88.7	72.8	261.9	23.3		7.2 ± 8.8	6.5 ± 3.9		−5.0 ± 20.7	−4.3 ± 20.2
	Subei (1)	E_3-N_1	39.5	94.7	69.0	327.8	3.7	15.4 ± 7.4	10.8 ± 8.1	7.3 ± 2.8	−33.9 ± 6.5	−29.3 ± 7.1	−28.8 ± 4.0
	Mahai (3)	E_{1-2l}-E_{3g}	38.4	94.3	63.4	211.2	9.9	15.2 ± 7.4	10.7 ± 8.0	10.1 ± 1.9	10.6 ± 10.5	15.1 ± 10.4	15.4 ± 8.7
	Tula (9)	K-E, E_3?	37.5	86.7	65.1	206.9	18.2	13.9 ± 7.5	12.1 ± 7.3	10.5 ± 1.8	9.3 ± 16.0	11.1 ± 15.9	12.7 ± 15.8
	Bulabashi (6)	J_{3k}	38.1	88.6	61.7	319.7	5.4*	11.2 ± 6.0	23.7 ± 9.8	19.1 ± 8.8	−34.0 ± 8.2	−46.5 ± 11.3	−41.9 ± 8.4
	Huatugou (4)	J_{3h},	38.5	90.6	50.1	197.2	7.3	24.4 ± 9.8	11.7 ± 6.0	19.1 ± 8.9	16.3 ± 9.7	29.0 ± 7.6	21.6 ± 9.4
	Lanzhou (H)	K_1	36.2	103.5	50.8	195.2	5.5	18.4 ± 7.7	13.6 ± 7.4	12.5 ± 2.6	26.4 ± 7.8	31.2 ± 9.6	32.3 ± 6.7
Tibet	Kekexili (5)	N_{1ch}	35.5	89.5	71.0	196.3	10.9		7.0 ± 8.5	6.2 ± 3.8		13.7 ± 12.0	14.5 ± 10.3
Tarim	Aksai (2)	E_{3b}	39.4	93.8	63.9	219.7	9.8		10.8 ± 8.1	10.6 ± 1.9		11.8 ± 10.4	12.0 ± 8.6
	Qiemo (8)	E-N?	38.1	86.6	75.8	229.5	9.6		7.6 ± 8.7	6.5 ± 3.9		1.9 ± 10.7	3.0 ± 9.1

Block	Reference Poles	λ_p (°N)	φ_p (°E)	A_{95} (°)	Reference
Tarim	J_3-K_1	64.6	208.9	9	*Li et al.* [1988]
	K	70.1	225.8	7	*Chen et al.* [1992]
	E_3-N_1	71.2	226.7	6.7	*Chen et al.* [1992]
NCB	J_3 (150 Ma)	75.9	223.6	5.3	*Gilder and Courtillot* [1997]; *Zhao et al.* [1990]
	K,	78.6	202.6	6.2	*Gilder and Courtillot* [1997]
	E (40Ma)	81.0	200.0		Estimated from *Gilder and Courtillot* [1997]
	N_2	83.8	199.4	7.1	*Gilder and Courtillot* [1997]
Eurasia	J_3 (150 Ma)	75.0	159.9	6.6	*Besse and Courtillot* [2001]
	K (70–130 Ma)	79.9	193.1	2.1	*Besse and Courtillot* [2001]
	E (30–50 Ma)	81.6	162.5	1.4	*Besse and Courtillot* [2001]
	N (15 Ma)	84.7	158.5	3.0	*Besse and Courtillot* [2001]
	N_2 (3 Ma)	86.3	166.6	2.5	*Besse and Courtillot* [2001]

[a] The λ and φ are latitude and longitude for the locality (l) and paleomagnetic pole (p), respectively; value with asterisk indicates mean calculated on specimen instead of site level. N_2, Upper Neogene (Plio-Pleistocene); N_1, Lower Neogene (Miocene); E_3, Oligocene; E_1, Paleocene; K_1, Lower Cretaceous; J_3, Upper Jurassic.

with few directions determined by principal component analysis, therefore, we consider it as a preliminary result. (e) Both the Neogene data from the valley south of Bulabashi and the data from Tula show considerable dispersion (α_{95} often >20°; Table 1) reflecting less stable magnetizations. Caution should be used when using these results. (f) Lower to Middle Jurassic data from the Bulabashi Coal Mine are clearly remagnetized as indicated by the negative fold test and the fact that the site mean directions in geographic coordinates are indistinguishable from the present Earth's field. (g) Five out of eight Jurassic block samples from Xorkol possess coherent inclinations in bedding-corrected coordinates but the declinations have random orientations, which is probably related to strong deformation of the rocks. We omit the Xorkol data from further discussion. (h) The Neogene data from Tibet (Kekexili) are not of good quality. They do pass the fold test, however, and as the rocks come from such a remote area, it is not likely that the data will be superseded in the near future.

4.2. Tectonic Interpretations

[33] In order to place the paleomagnetic data in a tectonic framework, we compared our data from the Qaidam Basin with coeval reference poles from the Tarim Basin, the North China Block (NCB) and Eurasia over time segments of Upper Jurassic (160 to 140 Ma), Cretaceous (130 to 70 Ma), Paleogene (64 to 24 Ma) and Neogene (24 to Present) (Table 2). We note that (1) the Paleogene NCB pole is interpolated from K and N_2 poles (which are similar) and (2) more thorough field studies of the Yingjisha section [*Chen et al.*, 1992] suggest that the paleomagnetic data assigned to the Cretaceous are actually Oligo-Miocene (E_3–N_1) (Table 2). With these caveats in mind, we calculated rotation angles for each of the relevant studies (Table 2 and Figure 5). We also note that as the paleomagnetic data base in central Asia grows, several research teams are discovering much shallower (∼20°) than expected inclinations (and thus paleolatitudes). While the shallow inclinations can reflect that the rock has been transported from more southerly latitudes than expected (i.e., the inclinations have tectonic significance), they can also arise by an aberration of the recording process that deflects the ''true'' geomagnetic field inclination toward the horizontal during sedimentation or compaction (thus giving ''false'' tectonic significance). Several hypotheses have been proposed to explain the origin of the shallow inclinations such as synsedimentary or compaction-induced inclination shallowing, tilted axial dipole, non-dipolar geomagnetic field geometry, tectonic shortening, tectonic escape, remagnetization, and non-rigidity of the Eurasian plate [*Chen et al.*, 1992, 1993, 2002; *Pozzi and Feinberg*, 1991; *Thomas et al.*, 1994; *Westphal*, 1993; *Bazhenov et al.*, 1994; *Cogné et al.*, 1999; *Chauvin et al.*, 1996; *Gilder et al.*, 1996, 2001; *Kodama and Tan*, 1997; *Halim et al.*, 1998]. Below we

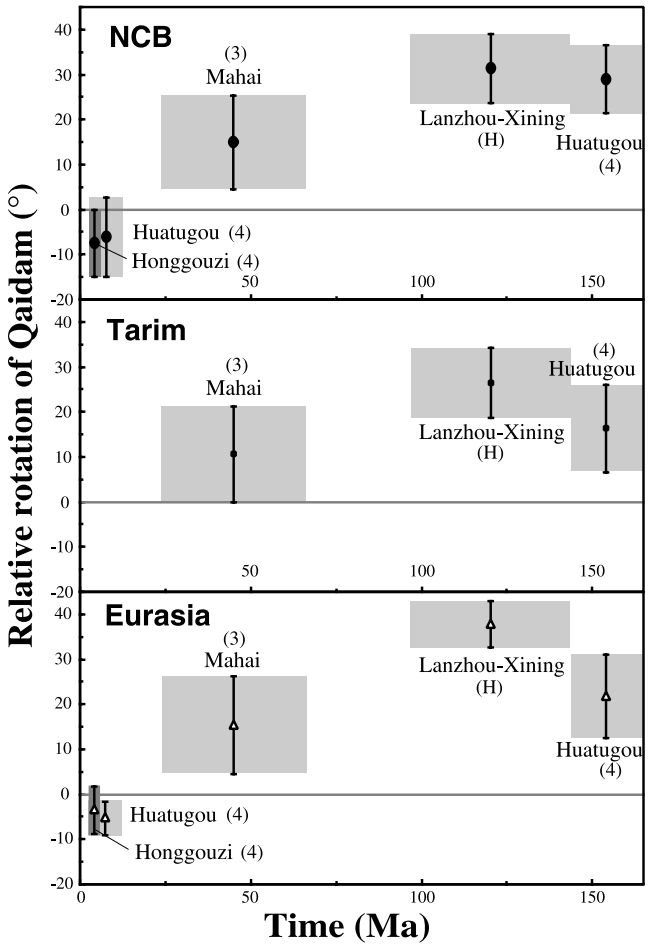

Figure 5. Relative rotation of Qaidam with respect to the NCB, Tarim Basin and Eurasia as a function of estimated time span of the rocks sampled (data from Table 2- gray shading represents field of age and rotation uncertainty). Studies <20 Ma are not compared to the Tarim Basin due to lack of reference pole. The number or letter in parentheses corresponds to the sampling area indicated in Figure 1b. Positive (negative) values for the relative rotation indicate clockwise (counterclockwise) rotation of the Qaidam Basin with respect to the reference block.

draw tectonic conclusions based solely on the rotation data, calculated following *Coe et al.* [1985], which should be largely immune from syn-sedimentary or compaction effects.

[34] Although each sample locality has been assigned to a specific tectonic block (such as Subei and Huatugou to the Qaidam Basin), it is probable that the blocks likely suffered internal deformation and have not behaved completely rigidly over long distances. The various mountain ranges within the Qaidam Basin suggest that the basement is cut by thrust faults, and thus each crustal sliver potentially deforms (and rotates) independently. However, the pattern of the rotations in space and time can yield information on the sense and age of motion.

[35] Localities that display significant counterclockwise rotation include the Oligo-Miocene Subei section ($-27° \pm 4°$), which is situated near the eastern part of the Altyn Tagh fault (95°E longitude) and the Upper Jurassic Bulabashi sequence ($-38° \pm 4°$) from the middle part (89°E longitude) (Figures 1 and 6; Table 2). Because these two localities lie within a few kilometers of the Altyn Tagh fault, we believe their counterclockwise rotations are local in nature and either represent rotated blocks within the shear zone (Bulabashi) or are related to drag near the shear zone (Subei). As the magnetostratigraphic study of Subei places it within the time interval from 26 Ma to 19 Ma, the rotation there is clearly younger than 19 Ma.

[36] Besides Subei and Bulabashi which underwent counterclockwise rotations, the other localities show either no significant rotation or significant clockwise rotation depending on their age and tectonic affiliation. In the Huatugou area (Figure 2), we obtained reliable data from both Upper Jurassic and Neogene sediments. The paleomagnetic directions of the Upper Jurassic red beds are rotated significantly clockwise $40° \pm 5°$ with respect to the overlying Neogene strata. Compared against the Tarim, NCB and Eurasian reference poles, the Upper Jurassic units are rotated clockwise $16.3° \pm 9.7°$, $29.0° \pm 7.6°$ and $21.6° \pm 9.4°$ respectively; whereas the Upper Miocene to Pleistocene yellow sandstones from Huatugou are rotated slightly counterclockwise ($-7.5° \pm 7.4°$ and $-5.3° \pm 3.9°$) with respect to the NCB and Eurasian reference poles. The Plio-Pleistocene Youshashan formation at Honggouzi, which lies about 30 km closer to the Altyn Tagh fault than Huatugou, is insignificantly rotated $-6.1° \pm 8.8°$ and $-3.4° \pm 6.2°$, again relative to the NCB and Eurasian reference poles. Thus, in the Huatugou area we document the existence of (1) negligible or very slight counterclockwise rotation since the Upper Miocene and (2) significant clockwise rotation between the Late Jurassic and the Upper Miocene.

[37] Besides the Upper Jurassic sediments from Huatugou, other localities from the Qaidam Basin display clockwise rotations (Figures 5 and 6). At Mahai, in the interior of the Qaidam Basin, the Paleogene (E_1 to E_3) red beds are rotated clockwise $10.6° \pm 10.5°$, $15.1° \pm 10.4°$ and $15.4° \pm 8.7°$ with respect to the Tarim, NCB and Eurasian reference poles. Cretaceous rocks from ten sites in the northeastern Qaidam Basin also show significant clockwise rotations of $26.4° \pm 7.8°$, $31.2° \pm 9.6°$ and $32.3° \pm 6.7°$ (Figure 6, locality H) [*Halim et al.*, 1998). These results are similar to those reported by *Yang et al.* [2001] whose sampling sites are close to those of *Halim et al.* [1998].

[38] Although these data represent a meager coverage of the Qaidam Basin, and more data may paint a more complicated history in detail [*Dupont-Nivet et al.*, 2000], we think that they impose significant constraints on the rotation of the Qaidam Basin and hence movement along the Altyn Tagh fault. Figure 5 shows the paleomagnetic rotations of the Qaidam localities with respect to the NCB, Tarim and Eurasia as a function of time. Taken together, the data in the figure show that J_3 to E_3 strata are rotated clockwise on the order of $20° \pm 5°$ with respect to the Tarim

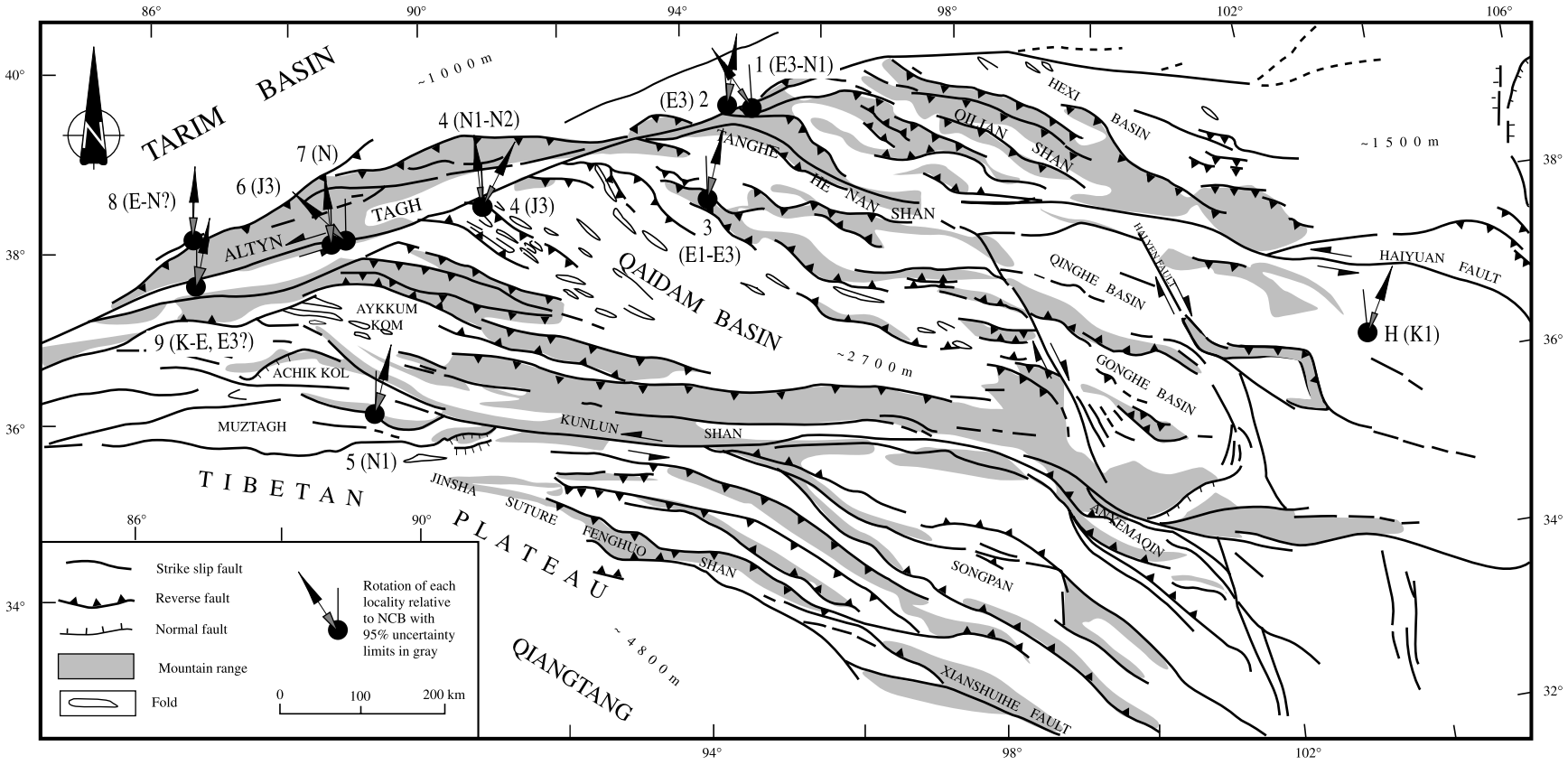

Figure 6. Tectonic map of the Qaidam Basin and surrounding region [after *Meyer et al.*, 1998]. The arrows show paleomagnetic rotations with respect to the NCB with uncertainties in gray (data from Table 2). The localities are: 1, Subei; 2, Aksai; 3, Mahai; 4, Huatugou+Honggouzi (N) and Huatugou (J3); 5, Kekexili; 6, Bulabashi; 7, Valley; 8, Qiemo; 9, Tula. H is the Lower Cretaceous sampling locality of *Halim et al.* [1998]. N2, Upper Neogene (Plio-Pleistocene); N1, Lower Neogene (Miocene); E3, Oligocene; E1, Paleocene; K1, Lower Cretaceous; J3, Upper Jurassic.

Basin, the NCB, and Eurasia, while Upper Miocene to Pleistocene rocks show no significant clockwise rotation. If Huatugou is indeed representative of the Qaidam Basin, as no major tectonic structure separates this area with the interior of the Qaidam Basin, it would suggest that the rotation of the Qaidam Basin occurred mostly from the latest Oligocene to the Upper Miocene, after deposition of the youngest sediments that are clockwise rotated, e.g., the Oligocene Lower Gachaigou formation from Mahai.

[39] One could argue that the deformation was partitioned and that the ~20° rotation is an artifact of insufficient sampling. For example, *Meyer* [1991] interpreted changes in slip rates along the Altyn Tagh fault from SW to NE as evidence for fault propagation. This is consistent with analog experiments using plasticine [*Tapponnier et al.*, 1982; *Peltzer and Tapponnier*, 1988] and plate velocity computations [*Replumaz*, 1999] which show the deformation propagating from the SW to the NE. Moreover, heterogeneous deformation within the Qaidam Basin is clear when observing its detailed topography and structural make up (Figures 1 and 6). Despite such evidence, if one assumes that the rotation pattern observed at Huatugou is representative of the Qaidam block, then the main phase of rotation, and strike-slip motion on the Altyn Tagh fault, began prior to the Upper Miocene, independent of the details of internal deformation of the Qaidam block itself. The same conclusion might also hold true for the Bulabashi area where Upper Jurassic rocks are rotated significantly counterclockwise, whereas the nearby Neogene units show no significant rotation (Figure 6, localities 6 and 7).

[40] Stratigraphic sections or distinct lithologic units that crop out on opposite sides of faults are commonly used to quantify the amount and sense of offset. It should be remembered, however, that this procedure is subject to large uncertainty, for basins or other geologic markers located several hundreds of kilometers apart could have formed in a similar tectonic environment and involve similar stratigraphies, genesis, etc., without ever having been offset by a fault. Despite this, several workers have used this (necessary but not sufficient) approach to estimate slip amounts on the Altyn Tagh fault. A 700 km displacement along the Altyn Tagh fault was proposed based on matching Paleozoic rock assemblages in the northeastern Kunlun and the western Pamir [*Tapponnier et al.*, 1981]. *Ritts and Biffi* [2000] proposed 400 ± 60 km of left-lateral offset on the Altyn Tagh fault following analyses on sedimentary facies, paleocurrent directions, sandstone compositions and biostratigraphies of Jurassic rocks from both sides of the fault. $^{40}Ar/^{39}Ar$ and apatite fission track thermochronologic data from two localities of Paleozoic rocks that lie on both sides of the fault, ~350 km apart, have similar Middle Jurassic cooling histories, which led *Sobel et al.* [2001] to suggest that 350 km of sinistral offset occurred along the Altyn Tagh fault after the Middle Jurassic. *Wang* [1997] correlated Oligocene sediments on both sides of the Altyn Tagh fault, near its eastern terminus, and concluded that it had been active from the Oligocene to the Present with about 60 km of sinistral offset.

[41] Correlation and dating (^{14}C, ^{10}Be, etc.) of offset geomorphic features suggest slip rates along the fault over the past 10–20 Myr are up to ~30 mm/yr in the west and taper eastward to ~5 mm/yr [*Peltzer et al.*, 1989; *Meyer et al.*, 1998; *Métivier et al.*, 1998; *Mériaux et al.*, 2000]. Satellite image analysis and field observations of the area east of 90°E led *Meyer et al.* [1998] to propose a minimum of 156 ± 40 km of sinistral displacement since 10 Ma. A study dating offset terraces and push-up structures with cosmogenic radionucleides on the Aksai-Subei segment (94°E) of the Altyn Tagh fault suggests a rate of 15 mm/yr, with a minimum bound of 12.5 mm/yr [*Mériaux et al.*, 2000]. Assuming the minimum slip rates are indicative for the past 24 Ma, the accumulated displacement along Altyn Tagh cannot be less than 300 km.

[42] Assuming the 20° clockwise rotation of the Qaidam Basin is a valid estimate, it can be used to constrain the quantity of slip along the Altyn Tagh fault. This is a major transcurrent fault that cuts through the entire lithosphere, as suggested by recent seismological profiles [*Wittlinger et al.*, 1998]. If the Euler pole representing Tarim-Qaidam rotation lies at 25°N and 92°E (obtained by fitting a small circle to the Altyn Tagh fault; Figure 1a), and assuming the Qaidam Basin rotated as a single rigid block, a 20° ± 5° rotation of the Qaidam Basin represents 500 ± 130 km of left-lateral offset. This is a maximum value as Qaidam surely experienced internal deformation. Moreover, the present paleomagnetic data also constrain the time of peak motion to be within ~24 Ma and ~10 Ma, which translates into a rotational velocity of the Qaidam Basin to be 1.4° ± 0.4°/Myr. The paleomagnetically constrained rotation rate of the Qaidam Basin yields a time-averaged slip rate of 36 ± 9 mm/yr on the Altyn Tagh fault or 21 ± 5 from 24 Ma to the present.

[43] Not only does the pattern of paleomagnetic rotations suggest that deformation was active in the 24 Ma to 10 Ma time window but other evidence exists as well. In a detailed study of the rock magnetic signature of the 2000 m thick Subei section, *Gilder et al.* [2001] found that the magnetite concentration in the rocks stayed constant from 26 to 23 Ma then, beginning at 23 Ma, magnetite abundance began to steadily increase. Their preferred explanation for the change was that magnetite-rich source rocks originally became exposed and eroded around 23 Ma, and that their exposure and concomitant erosion amplified until at least 19 Ma, which is the top of the studied section. At Subei, the anisotropy of magnetic susceptibility shape parameter also varies systematically with depth. From 26 to 21 Ma, the magnetic ellipsoids are spherical on average then beginning at 21 Ma, they become notably oblate. Well-rounded particles in the relatively fine-grained part of the sequence likely reflect that the grains were relatively far traveled. The change to oblate ellipsoids occurs when the coarse conglomerate beds become dominant. Both the large clast sizes (>1 m) and oblate AMS shapes in these beds probably indicate that the source was in close proximity to the deposition center. *Gilder et al.* [2001] interpreted this change at 21 Ma to reflect rapid uplift of a source near Subei, which

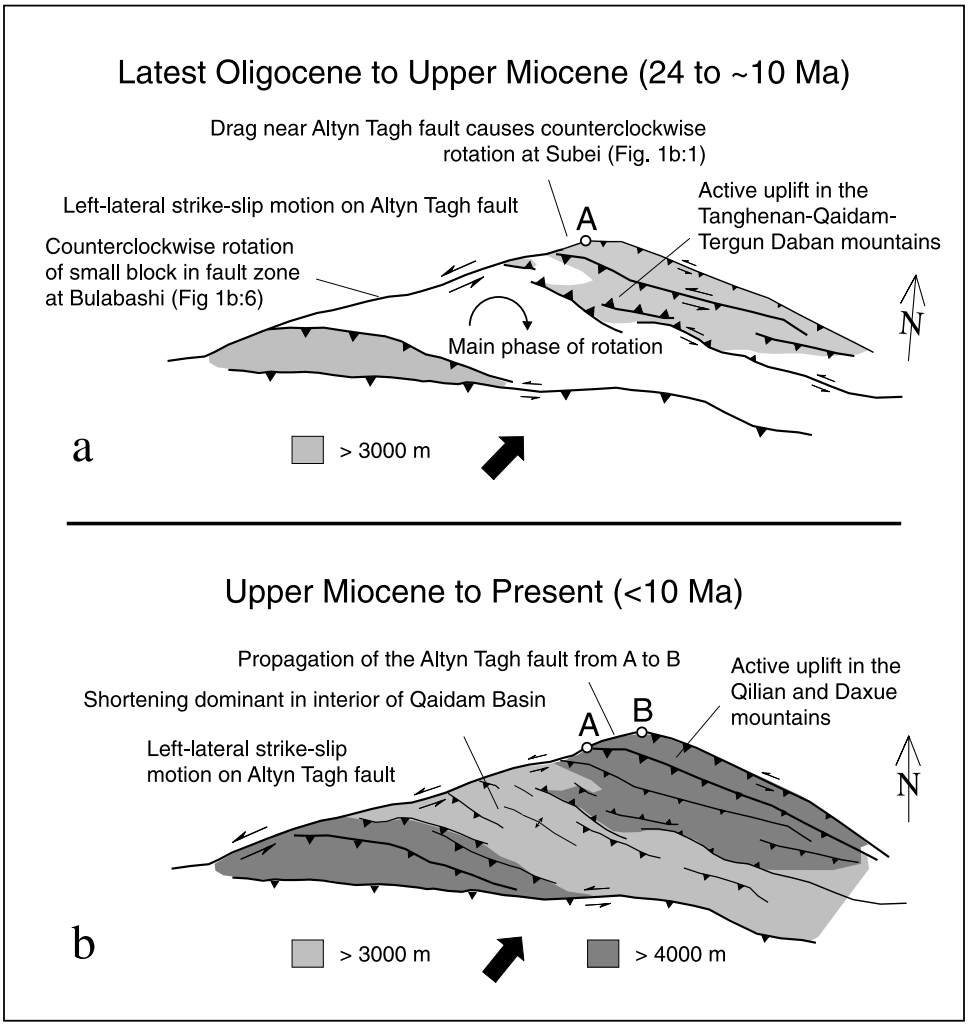

Figure 7. Two-stage model of the tectonic evolution of the Qaidam Basin and Altyn Tagh fault. (a) From the latest Oligocene to the Upper Miocene the Qaidam Basin undergoes significant clockwise rotation. Rotation is accommodated by left-lateral shear along the Altyn Tagh fault and by shortening accommodated in the Tergun Daban, Qaidam and Tanghenan mountains. (b) From the Upper Miocene to Present, deformation becomes increasingly important in the interior of the Qaidam Basin. Propagation of the Altyn Tagh fault farther northeast is accompanied by uplift in the Daxue and Qilian mountains.

was possibly the Tanghenan or Tergun Daban mountains to the south. Thus the rock magnetic profiles can be interpreted to suggest that mountain building was active in the Subei area as early as 23 to 21 Ma. Other workers have also found evidence for active mountain building to occur in the region around this time, including (1) the commencement of unroofing found in apatite fission track dates along the central part of the Altyn Tagh fault near Huatugou (19 ± 1 Ma, 20 ± 2 Ma and 22 ± 2 Ma [*Sobel et al.*, 2001]), and from the Tian Shan (~24 Ma [*Hendrix et al.*, 1994]), and Kunlun ranges (25 Ma to 13 Ma [*Sobel and Dumitru*, 1997]), and (2) the start of rapid continental sedimentation in the Tarim Basin at about 22 Ma [*Métivier and Gaudemer*, 1997]. Recent fission track dating in the northern Qilian mountains also shows evidence for a cooling episode between 20 Ma and 10 Ma [*George et al.*, 2001].

[44] Figure 7 presents a simple model to clarify how our findings relate to the kinematic evolution of the Qaidam Basin - Altyn Tagh fault system. The model suggests that the Altyn Tagh fault was most active in the latest Oligocene to Upper Miocene when it propagated from the Kunlun to ~94°E, northwest of the Tergun Daban, Qaidam and Tanghenan mountains (Figure 7a). This is consistent with a marked Neogene, yet pre-Pliocene, deformation event observed in the Tergun Daban range (P. Tapponnier, personal communication, 2001). We thus suggest that the bulk of the shortening and rotation of the Qaidam Basin was accommodated in the Tergun Daban, Qaidam and Tanghenan mountains, which is consistent with the observation

that the highest topography in the northeastern Qaidam Basin lies there (Figure 1b). *Avouac and Tapponnier* [1993] argued that the Tian Shan mountains formed by relative rotation between the Junggar and Tarim blocks based on the observation that the 3000 m contour of the Tian Shan widens to the west. We note that the high topography in the northeastern Qaidam Basin also widens to the west (Figure 1b), which is probably a consequence of differential shortening during counterclockwise rotation of the various crustal slivers in Qaidam that produces more shortening in the west than in the east. We imagine that the Qaidam region looked in the Early Miocene like the Tian Shan looks today—a high mountain range to the north, separated from the Kunlun Mountains to the south by a low, broad basin (like the Tarim Basin) that underwent comparatively little internal deformation. After the main phase of rotation and displacement on the Altyn Tagh fault occurred, continued India-Asia convergence and related shortening led to (1) propagation of the Altyn Tagh fault farther east, (2) the building of the Daxue and Qilian mountains, and (3) heightened deformation within in the interior of the Qaidam Basin (Figure 7b). This two-stage model is superior to one based on continuous propagation of the Altyn Tagh fault because the latter (1) cannot explain why mountain building was active in the northeastern Qaidam Basin as early as 23 Ma, (2) is inconsistent with the topographic profile of the Qaidam Basin, and (3) does not match in time with the pattern of paleomagnetic rotations.

5. Conclusions

[45] The present paleomagnetic study carried out in the Qaidam and Tarim basins and in northern Tibet shows that central Asia has suffered heterogeneous deformation over different length scales. Localities close to the Altyn Tagh fault, such as Subei and the Bulabashi coal mine, display episodic, important counterclockwise rotations that confirm the left-lateral sense of motion along this fault. Locations farther away from the fault and in the interior of the Qaidam Basin, however, suggest that the left-lateral slip on the Altyn Tagh fault was accommodated by a roughly 20° clockwise rotation of the Qaidam Basin between about 24 Ma and 10 Ma. This time period coincides with heightened sedimentation rates, apatite fission track cooling ages and changes in sediment source characteristics found in the region — both along the Altyn Tagh fault and in the mountains of northeastern Qaidam. From the 20° clockwise rotation, we estimate some 500 km of offset occurred along the Altyn Tagh fault at a mean slip rate of 36 ± 9 mm/yr.

[46] **Acknowledgments.** This study was part of French-Chinese Altyn Tagh cooperative project supported by French geoscience organization INSU-CNRS and the Ministry of Geology of China. We thank B. Meyer, E. Sobel and P. Tapponnier for valuable discussions, A. Hanson and B. Ritts, for providing reprints and details on ages of particular sections, and Z. Yang for helpful suggestions. Chris Klootwijk and an anonymous reviewer contributed very helpful comments. IPGP contribution 1800.

References

Avouac, J.-P., and P. Tapponnier, Kinematic model of active deformation in Central Asia, *Geophys. Res. Lett.*, *20*, 1791–1798, 1993.

Bazhenov, M. L., H. Perroud, A. Chauvin, V. S. Burtman, and J. C. Thomas, Paleomagnetism of Cretaceous red beds from Tadzhikistan and Cenozoic deformation due to India-Eurasia collision, *Earth Planet. Sci. Lett.*, *124*, 1–18, 1994.

Besse, J., and V. Courtillot, Apparent and true polar wander and the geometry of the geomagnetic field for the last 200 Myr, *J. Geophys. Res.*, *107*, 10.1029/2000JB000050, in press, 2002.

Bureau of Geology and Mineral Resources of Gansu Province (BGMRGP), Regional Geology of Gansu Province, *Geol. Mem. Geol. Surv. China, Ser. 1*, *19*, 691 pp., 1989.

Bureau of Geology and Mineral Resources of Qinghai Province (BGMRQP), Regional geology of Qinghai Province, *Geol. Mem. Geol. Surv. China, Ser. 1*, *24*, 662 pp., 1991.

Bureau of Geology and Mineral Resources of Xinjiang Uygur Autonomous Region (BGMRXUAR), Regional geology of Xinjiang Uygur Autonomous Region, *Geol. Mem. Geol. Surv. China, Ser. 1*, *32*, 841 pp., 1993.

Chauvin, A., H. Perroud, and M. L. Bazhenov, Anomalous low paleomagnetic inclinations from Oligocene-Lower Miocene red beds of the south-west Tien Shan, Central Asia, *Geophys. J. Int.*, *126*, 303–313, 1996.

Chen, Y., J.-P. Cogné, and V. Courtillot, New paleomagnetic poles from the Tarim Basin, northwestern China, *Earth Planet. Sci. Lett.*, *114*, 17–38, 1992.

Chen, Y., V. Courtillot, J. P. Cogné, J. Besse, Z. Y. Yang, and R. Enkin, The configuration of Asia prior to the collision of India: Cretaceous paleomagnetic constraints, *J. Geophys. Res.*, *98*, 21,927–21,941, 1993.

Chen, Y., H. Wu, V. Courtillot, and S. Gilder, Large NS convergence at the northern edge of the Tibetan plateau?: New Early Cretaceous paleomagnetic data from Hexi Corridor, NW China, *Earth Planet. Sci. Lett.*, *201*, 293–307, 2002.

Chen, Z., N. Wu, D. Zhang, J. Hu, G. Shen, G. Wu, H. Tang, and Y. Hu, Geological map of the Xinjing Uygur Autonomous Region, China, scale 1:2,000,000, Geol. Publ. House, Bejing, 1985.

Coe, R. S., B. R. Globerman, P. W. Plumley and G. A. Thrupp, Paleomagnetic results from Alaska and their tectonic implications, in *Tectonostratigraphic Terranes of the Circum-Pacific Region*, *Earth. Sci. Ser.*, vol. 1, edited by D. G. Howell, pp. 85–108, Circum-Pac. Counc. for Energy and Miner. Resour., Houston, Tex., 1985.

Cogné, J. P., N. Halim, Y. Chen, and V. Courtillot, Resolving the problem of shallow magnetizations of Tertiary age in Asia: Insights from paleomagnetic data from the Qiangtang, Kunlun, and Qaidam blocks (Tibet, China), and a new hypothesis, *J. Geophys. Res.*, *104*, 17,715–17,734, 1999.

Dupont-Nivet, G., R. F. Butler, and A. Yin, Preliminary paleomagnetic results from Tertiary strata adjacent to the Altyn Tagh fault, *Eos Trans*, *81*(48), Fall Meet. Suppl., Abstract T62D-092000.

Fisher, R. A., Dispersion on a sphere, *Proc. R. Soc London., Ser. A*, *217*, 295–305, 1953.

George, A. D., S. J. Marshallsea, K. H. Wyrwoll, J. Chen, and Y. C. Lu, Miocene cooling in the northern Qilian Shan, northeastern margin of the Tibetan Plateau, revealed by apatite fission-track and vitrinite-reflectance analysis, *Geology*, *29*, 939–942, 2001.

Gilder, S., and V. Courtillot, Timing of the North-South China collision from new middle to late Mesozoic paleomagnetic data from the North China Block, *J. Geophys. Res.*, *102*, 17,713–17,727, 1997.

Gilder, S. A., X. X. Zhao, R. S. Coe, Z. F. Meng, V. Courtillot, and J. Besse, Paleomagnetism, tectonics and geology of the southern Tarim basin, northwestern China, *J. Geophys. Res.*, *101*, 22,015–22,031, 1996.

Gilder, S., Y. Chen, and S. Sen, Oligo-Miocene magnetostratigraphy and environmental magnetism of the Xishuigou section, Subei (Gansu Province, western China): Further implication on the shallow inclination of central Asia, *J. Geophys. Res.*, *106*, 30,505–30,521, 2001.

Halim, N., J.-P. Cogné, Y. Chen, R. Atasiei, J. Besse, V. Courtillot, S. Gilder, J. Marcoux, and R. Zhao, New Cretaceous and Early Tertiary paleomagnetic results from Xining-Lanzhou basin, Kunlun and Qiangtang blocks, China: Implications on the geodynamic evolution of Asia, *J. Geophys. Res.*, *103*, 21,025–21,045, 1998.

Halim, N., Y. Chen, J. P. Cogné, and S. Gilder, A first paleomagnetic study of Jurassic formations from the Qaidam Basin, Northeastern Tibet, China—Tectonic implications, *Geophys. J. Int.*, in press, 2002.

Halls, H. C., The use of converging remagnetization circles in paleomagnetism, *Phys. Earth Planet. Int.*, *16*, 1–11, 1978.

Hendrix, M. S., T. A. Dumitru, and S. A. Graham, Late Oligocene-early Miocene unroofing in the Chinese Tian Shan: An early effect of the India-Asia collision, *Geology*, *22*, 487–490, 1994.

Kirschvink, J. L., The least squares line and the analysis of paleomagnetic data, *Geophys. J. R. Astron Soc.*, *62*, 699–718, 1980.

Kodama, K. P., and X. Tan, Central Asian inclination anomalies: Possible inclination shallowing in red beds? (abstract), *Eos Trans.*, *78*(46), Fall Meet. Suppl., F1741997.

Li, Y. P., Z. Zhang, M. McWilliams, R. Sharps, Y. Zhai, Y. A. Li, Q. LI, and A. Cox, Mesozoic paleomagntic

results of the Tarim craton: Tertiary relative motion between China and Siberia?, *Geophys. Res. Lett.*, *15*, 217–220, 1988.

Lockley, M. G., B. D. Ritts, and G. Leonardi, Mammal track assemblages from the Early Tertiary of China, Peru, Europe and North America, *Palaios*, *14*, 398–404, 1999.

McElhinny, M. W., Statistical significance of the fold test in paleomagnetism, *Geophys. J. R. Astron. Soc.*, *8*, 338–340, 1964.

McFadden, P. L., and F. J. Lowes, The discrimination of mean directions drawn from Fisher distributions, *Geophys. J. R. Astron. Soc.*, *67*, 19–33, 1981.

McFadden, P. L., and M. McElhinny, The combined analysis of remagnetization circles and direct observations in paleomagnetism, *Earth Planet. Sci. lett.*, *87*, 152–160, 1988.

McFadden, P., and M. McElhinny, Classification of the reversal test in paleomagnetism, *Geophys. J. Int.*, *130*, 725–729, 1990.

Mériaux, A., F. Ryerson, P. Tapponnier, J. Van der Voerd, R. Finkel, M. Caffee, C. Lasserre, X. Xu, H. Li, and Z. Xu, Fast extrusion of the Tibet Plateau: A 3cm/yr, 100 kyr slip-rate on the Altyn Tagh fault, *Eos Trans.*, *81*(48), Fall Meet. Suppl., Abstract T62D-07, 2000.

Métivier, F., and Y. Gaudemer, Mass transfer between eastern Tien Shan and adjacent basins (central Asia): Constraints on regional tectonics and topography, *Geophys. J. Int.*, *128*, 1–17, 1997.

Métivier, F., Y. Gaudemer, P. Tapponnier, and B. Meyer, Northeastward growth of the Tibet Plateau deduced from balanced reconstruction of two depositional areas: The Qaidam and Hexi basins, China, *Tectonics*, *17*, 823–842, 1998.

Meyer, B., Mécanisme des grands tremblements de terre et du raccourcissement crustal oblique au bord nord-est du Tibet, Ph.D. thesis, Univ. Paris VI, 1991.

Meyer, B., P. Tapponnier, L. Bourjot, F. Métivier, Y. Gaudmer, G. Peltzez, S. Gou, and Z. Chen, Crustal thickening in Gansu-Qinghai, Lithospheric mantle subduction, and oblique, strike-slip controlled growth of the Tibet Plateau, *Geophys. J. Int.*, *135*, 147, 1998.

Molnar, P., and P. Tapponnier, Active tectonics of Tibet, *J. Geophys. Res.*, *93*, 5361–5375, 1978.

Peltzer, G., and P. Tapponnier, Formation and evolution of strike-slip faults and basins during the India-Asia collision: An experimental approach, *J. Geophys. Res.*, *93*, 15,085–15,117, 1988.

Peltzer, G., P. Tapponnier, and R. Armijo, Magnitude of late Quaternary left-lateral displacements along the northern edge of Tibet, *Science*, *246*, 1285–1289, 1989.

Pozzi, J. P., and H. Feinberg, Paleomagnetism in the Tajikistan: Continental shortening of European margin in the Pamirs during Indian Eurasian collision, *Earth Planet. Sci. Lett.*, *103*, 365–378, 1991.

Replumaz, A., Reconstruction de la zone de collision Inde-Eurasie, Etude centrée sur l'Indochine, Ph. D. thesis, Univ. Paris VII, 1999.

Ritts, B. D., and U. Biffi, Magnitude of post Middle Jurassic (Bajocian) displacement on the Altyn Tagh fault, NW China, *Geol. Soc. Am. Bull.*, *112*, 61–74, 2000.

Ritts, B., A. Hanson, D. Zinniker, and M. Moldowan, Lower-Middle Jurassic nonmarine source rocks and petroleum system of the northern Qaidam basin, northwest China, *AAPG Bull.*, *83*, 1980–2005, 1999.

Rumelhart, P., A. Yin, E. Cowgill, R. Butler, Z. Qing, and X. Wang, Cenozoic vertical axis rotation of the Altyn Tagh fault system, *Geology*, *27*, 819–822, 1999.

Sobel, E. R., and T. A. Dumitru, Thrusting and exhumation around the margins of the western Tarim basin during the India-Asia collision, *J. Geophys. Res.*, *102*, 5043–5063, 1997.

Sobel, E. R., N. Arnaud, M. Jolivet, B. D. Ritts, and M. Brunel, Jurassic to Cenozoic exhumation history of the Altyn Tagh range, NW China constrained by $^{40}Ar/^{39}Ar$ and apatite fission track thermochronology, in *Paleozoic and Mesozoic Tectonic Evolution of Central and Eastern Asia*: *From Continental Assembly to Intracontinental Deformation*, edited by M. S. Hendrix and G. A. Davis, *Mem. Geol. Soc. Am., 194*, 454 pp., 2001.

Tapponnier, P., M. Mattauer, F. Proust, and C. Cassaigneau, Mesozoic ophiolites, sutures and large-scale tectonic mouvement in Afghanistan, *Earth Planet. Sci. Lett.*, *52*, 355–371, 1981.

Tapponnier, P., G. Peltzer, R. Armijo, A. La Dain, and P. Cobbold, Propagating extrusion tectonics in Asia: New insights from simple experiments with plasticine, *Geology*, *10*, 611–616, 1982.

Tapponnier, P., et al., Active thrusting and folding in the Qi Lian Shan, and decoupling between the upper crust and mantle in northern Tibet, *Earth Planet. Sci. lett.*, *97*, 382–403, 1990.

Tapponnier, P., Z. Q. Xu, F. Roger, B. Meyer, N. Arnaud, G. Wittlinger, and J. S. Yang, Oblique stepwise rise and growth of the Tibet plateau, *Science*, *294*, 1671–1677, 2001.

Thomas, J. C., A. Chauvin, D. Gapais, M. L. Bazhenov, H. Perroud, P. R. Cobbold, and V. S. Burtman, Paleomagnetic evidence for Cenozoic block rotations in the Tadjik depression (central Asia), *J. Geophys. Res.*, *99*, 15,141–15,160, 1994.

Wang, E., Displacement and timing along the northern strand of the Altyn Tagh fault zone, Northern Tibet, *Earth Planet. Sci. lett.*, *150*, 55–64, 1997.

Westphal, M., Did a large departure from the geocentric axial dipole hypothesis occur during the Eocene?: Evidence from the magnetic polar wander path of Eurasia, *Earth Planet. Sci. Lett.*, *117*, 15–28, 1993.

Wittlinger, G., P. Tapponnier, G. Poupinet, M. Jiang, D. Shi, G. Herquel, and F. Masson, Tomographic evidence for localized lithospheric shear along the Altyn Tagh Fault, *Science*, *282*, 74–76, 1998.

Yang, T., Z. Yang, Z. Sun, and A. Lin, New Early Cretaceous paleomagnetic results from the Qilian orogenic belt and its tectonic implications, *Sci. China*, *44*, 568–576, 2001.

Yin, A., M. Harrison, M. Murphy, M. Grove, S. Nie, F. Ryerson, W. Feng, and Z. Le, Tertiary deformation history of southeastern and southwestern Tibet during the Indo-Asian collision, *Geol. Soc. Am. Bull*, *111*, 1644–1664, 1999.

Yin, A., Z. Yang, R. Butler, Y. Otofuji, P. E. Rumelhart, and E. Cowgill, Correction of "Cenozoic vertical-axis rotation of the Altyn Tagh fault system" by P. Rumelhart et al., *Geology,* v. 27, p. 819–822, September 1999, *Geology*, *28*, 480, 2000.

Zhao, X., R. S. Coe, Y. Zhou, H. Wu, and A. J. Wang, New paleomagnetic results from northern China: Collision and suturing with Siberia and Kazakhstan, *Tectonophysics*, *181*, 43–81, 1990.

Zijderveld, J. D., A. C. demagnetization of rocks: Analysis of results, in *Methods in Paleomagnetism*, edited by D. W. Collisson, K. M. Creer, and S. K. Runcorn, 245–286, Elsevier Sci., New York, 1967.

Y. Chan, Département des Sciences de la Terre, ISTO, Université d'Orléans, F-45067 Orléans cedex 02, France. (Yan.Chen@univ-orleans.fr)

J.-P. Cogné, V. Courtillot, and S. Gilder, Laboratoire du Paléomagnétisme, Institut de Physique du Globe de Paris, 4 place Jussieu, F-75252 Paris cedex 05, France.

N. Halim, Laboratory of Paleomagnetism, Kobe University, Nada, 657-8501, Kobe, Japan.